Geochemistry of sands along the San Nicolás and San Carlos beaches, Gulf of California, Mexico: implications for provenance and tectonic setting

John S. ARMSTRONG-ALTRIN[1],*, Ramasamy NAGARAJAN[2], Yong Il LEE[3],
Juan J. KASPER-ZUBILLAGA[1], Leslie P. CÓRDOBA-SALDAÑA[4]

[1]Institute of Marine Sciences and Limnology, Unit of Ocean and Coastal Processes,
National Autonomous University of Mexico, Mexico City, Mexico
[2]Department of Applied Geology, School of Engineering and Science, Curtin University, Miri, Sarawak, Malaysia
[3]School of Earth and Environmental Sciences, Seoul National University, Seoul, South Korea
[4]Posgraduate Program in Marine Sciences and Limnology, National Autonomous University of Mexico, Mexico City, Mexico

Abstract: The weathering conditions, provenance, and tectonic setting of sands from the San Nicolás (SN) and San Carlos (SC) beaches along the Gulf of California, Mexico, have been studied using mineralogy, major element, and trace element data. The compositional similarity among 4 independent groups (each beach area consists of 2 grain-size groups, i.e. medium- and fine-grained sands) was tested statistically by the application of analysis of variance at the 99% confidence level to avoid misinterpretation. The X-ray diffraction and SEM-EDS data revealed that the fine-grained SN sands were abundant in rutile and zircon minerals. The higher SiO_2/Al_2O_3 ratio of the SN sands than the medium- and fine-grained SC sands indicated that the compositional maturity was greatest for the SN sands ($F_{calc} = 366.756151$ and $(F_{crit})_{99\%} = 5.065158$, where $F_{calc} > (F_{crit})_{99\%}$ indicates that the data populations are significantly different at 99% confidence level). The chemical index of alteration values for the SN (ca. 41–45) and SC (ca. 48–51) sands indicated low to moderate weathering intensity in the source region. The significant enrichment of the low rare earth element and the flat heavy rare earth element patterns of the SN sands indicated that the sources were largely felsic rocks. The low positive Eu anomaly in the SC sands was probably due to the contribution of sediments from intermediate rocks between felsic and mafic compositions. The comparison of rare earth element data of the sands with rocks located relatively close to the study areas revealed that the SN sands received a major contribution from felsic rocks and SC sands from intermediate rocks. The compositional difference between the SN and SC beach areas indicated that longshore currents played a less significant role. Discriminant function-based major element diagrams for the tectonic discrimination of siliciclastic sediments revealed a rift setting for the Gulf of California, which is consistent with the general geology of Mexico.

Key words: Beach sand, SEM-EDS, X-ray diffraction, weathering, rift setting, rare earth element

1. Introduction

Major and trace element composition of terrigenous sediments is considered as a valuable tool to identify the provenance and tectonic setting (Zhang et al., 2011; Concepcion et al., 2012; Srivastava et al., 2013). Several trace elements such as rare earth elements (REEs) Y, Th, Zr, Hf, Nb, and Sc are best suited for provenance study, because of their relatively low mobility during sedimentary processes and their short residence times in sea water (Cullers et al., 1979; Young et al., 2013). Numerous studies showed that major and trace elements can be added or subtracted from a rock during seawater–basalt interaction (Verma, 1992; Verma et al., 2005; Hofmann and Harris, 2008). A study carried out by Greenough et al. (1990) on geochemical effects of alteration on basalts from the Indian Ocean pointed out that REEs and elements like Zr, Nb, Y, Ti, Al, V,

Th, P, and Hf were immobile and Cu, Cr, and Zn were mobile during alteration processes. However, Torres-Alvarado et al. (2007) recently studied the effect of hydrothermal alteration on the chemistry of volcanic rocks from the Los Azufres geothermal field, Mexico, and found that most major elements and a few trace elements, including high field strength elements such as Zr, Ti, and P, were mobilized during hydrothermal alteration. They cautioned against the use of these elements for petrogenetic studies of igneous and metamorphic rocks. Although provenance studies are common (Hossain et al., 2010, 2014; Armstrong-Altrin and Natalhy-Pineda, 2013), studies focused on the geochemical variation in sediments with respect to grain size are meagre (e.g., Ohta, 2008; Effoudou-Priso, 2014).

The study areas of the San Nicolás (SN) and San Carlos (SC) beaches are located along the Gulf of California.

* Correspondence: armstrong@cmarl.unam.mx

The textural characteristics of the beach sands of the Gulf of California have been studied by Marsaglia (1991). Previous studies by Kasper-Zubillaga et al. (2008a, 2008b) addressed the geochemistry of the Puerto Peñasco and El Vizcaino dune sands of northwestern Mexico. Armstrong-Altrin (2009) studied the geochemistry of sediments from the Bahia Kino beach of the Gulf of California and concluded that the beach sands are a good indicator of the source rocks (Figure 1a). However, these studies were based on sand samples collected from a single beach and within a restricted geographic area, and they did not focus on the compositional differences with respect to grain size and tectonic setting.

The present study examines the mineralogy and geochemistry of sand samples collected from the beaches at SN and SC, Gulf of California (Figure 1). The objective of this study is to investigate the compositional difference between the 2 beach areas and to infer the provenance and tectonic environment. In addition, this study highlights the geochemical heterogeneity between the medium- and fine-grained sands.

2. Study area
The study areas, the SN and SC beaches, are located on the Gulf of California (28°42′28.33″N, 111°54′22.33″W and 27°57′42.24″N, 111°05′59.11″W, respectively),
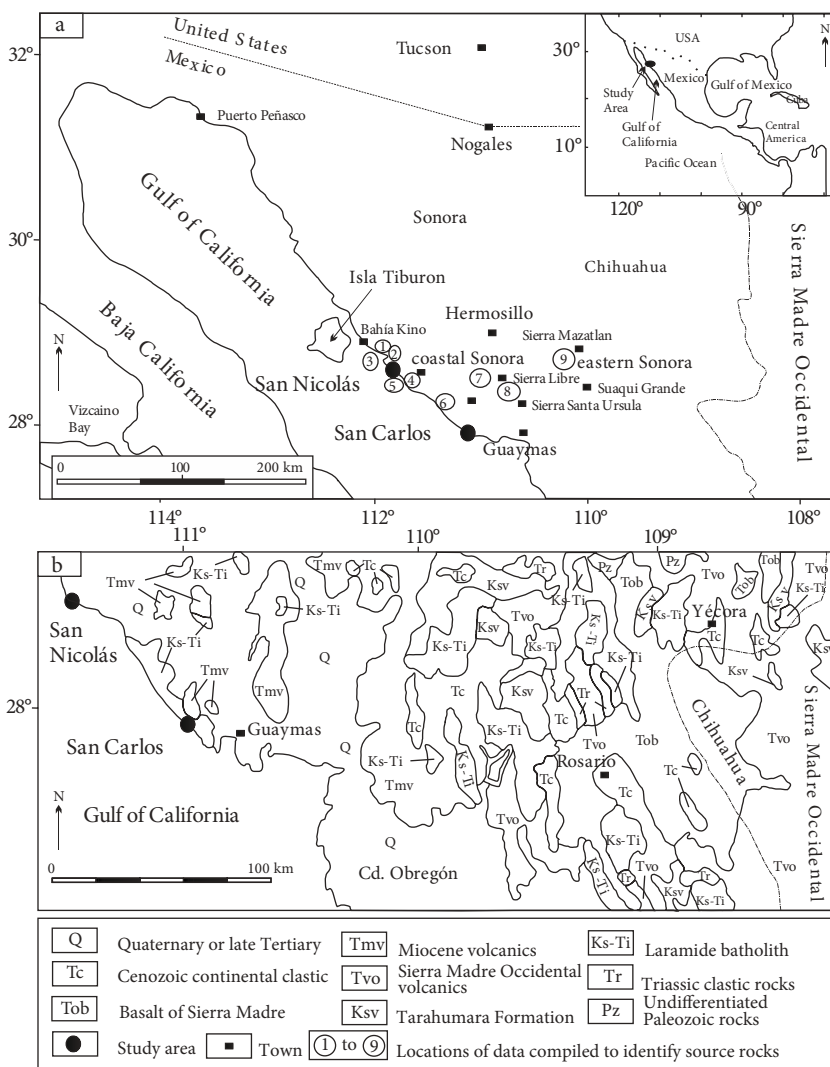
Figure 1. a) Map showing study areas and locations of the source areas from where the geochemical data were compiled for comparison (map modified after Till et al., 2009). 1. Vidal-Solano et al. (2007), 2. Valencia-Moreno et al. (2001), 3. Desonie (1992), 4. Valencia-Moreno et al. (2003), 5. Saunders (1983) and Saunders et al. (1982), 6. Roldán-Quintana et al. (2009), 7–9. Till et al. (2009). **b)** Simplified geology map of the study area (map modified after Roldán-Quintana et al., 2009).

in the northwestern part of Mexico (Figure 1a). The distance between the 2 beach areas is approximately 150 km. The coastal Sonora batholith, located in this part, is characterized by continuous exposures of early Cretaceous to early Tertiary granitic rocks along the NW-SE oriented belt (Valencia-Moreno et al., 2003). The exposed sedimentary rocks are early Jurassic quartz arenites, Tertiary sandstones, and Quaternary alluvium. The volcanic rocks are andesite and rhyolite types (Desonie, 1992; Vidal-Solano et al., 2007) of early Tertiary age. Among the intrusive rocks, granites and granodiorites of Mesozoic age are dominant (Figure 1b) (Valencia-Moreno et al., 2001, 2003). Major rivers that drain near the beach areas are absent. The study area of the Gulf of California is a classical example of a transition from an active continental margin to a regime of lithospheric extension resulting in the formation of a rift and the establishment of a new boundary between the Pacific Plate and the North American Plate (Paz-Moreno and Demant, 1999; Conly et al., 2005).

3. Analytical methods

Twenty surface sand samples were collected from the SN (n = 10) and SC (n = 10) beach areas. Grain size analysis was carried out with a Ro-Tap sieve shaker using American Society for Testing and Material sieves ranging from –1.5 □ to 4.25 □ at 0.50 □ intervals for 20 min (Folk, 1966). Cumulative curves were constructed to calculate the statistical grain size parameters (mean grain size and sorting values) by applying the equations of Folk and Ward (1957).

Fifteen thin sections were prepared for petrography study. Point counting (300 grains) was carried out following the Gazzi–Dickinson method (Dickinson et al., 1983; Ingersoll et al., 1984; Suttner and Basu, 1985). However, caution should be taken when following the Dickinson triangular diagram. Weltje (2006) tested the Dickinson model and pointed out that the provenance of mixed sands is likely to more accurately reflect the source rocks when the log-ratio transformation of the principal framework components is applied and 6 compositional frameworks [Qm (monocrystalline quartz), Qp (polycrystalline quartz), P, K, Lv, and Ls] are used. Besides this, the use of ternary diagrams was discouraged by Verma (2010, 2012) because of severe error distortion problems. More recently, a new modified methodology using a quantitative electron microscope scanner for assessing sandstone framework composition was recommended by Allen et al. (2012).

In this study, the major compositional framework grains counted are total quartz [Q = total quartz grains], total feldspar [F = K (potash feldspar) + P (plagioclase)], total lithic fragments [L = volcanic (Lv) + sedimentary (Ls) + metamorphic (Lm) + plutonic (Lp)], heavy minerals (HM), and biogenic components [B = shells, algae, and corals].

Ten sand grains from each sample were selected for scanning electron microscope (SEM) study at the Petrology Laboratory, Institute of Geophysics, National Autonomous University of Mexico (UNAM). The chemical composition of the sand grains was studied with a PHILLIPS XL-30 SEM equipped with an EDAX spectrometer (EDS) system. The mineralogy was studied using a Siemens D5000 X-ray diffractometer (XRD) at the X-ray fluorescence spectrometry (XRF) Laboratory, Institute of Geology, UNAM.

The major and trace elements were analyzed individually for the 20 medium-grained and 20 fine-grained sands, with 2 analyses per sample. Major elements for SN sands were analyzed using conventional XRF procedures at the Institute of Geology, UNAM. Powdered samples were heated to 110 °C for 6 h followed by heating in a muffle furnace at 1000 °C for 2 h to determine the loss on ignition (LOI). Lithium tetraborate was mixed with the powdered samples and heated to 1000 °C to form a fused sample for X-ray fluorescence analysis. Final analysis was carried out using a Rigaku model RIX-3000 equipped with a Rh tube. Calibration curves were prepared using international reference materials (Lozano and Bernal, 2005). Chemical analysis for major elements has precision of better than 5%. Major element data were recalculated to an anhydrous (LOI-free) basis and adjusted to 100% before using them in various diagrams.

The trace elements for the SN beach sands were determined by instrumental neutron activation analysis using an automated dual detector (GeLi for high energy gamma rays and LEGe for low energy gamma rays) system. US Geological Survey standards AGV-1 and SCo-1 were used for calibration and the analytical precision for trace elements and REEs is generally better than 5%.

The major and trace elements for the SC sands were analyzed at the Korea Basic Science Institute, Daejeon, South Korea. Major elements were analyzed by XRF spectrometry. Trace element (Ba, Co, Cr, Cu, Ni, Sc, Sr, V, Zn, and Zr) concentrations were determined using a Jobin Yvon 138 Ultrace inductively coupled plasma atomic emission spectrometer. The REEs Cs, Hf, Nb, Pb, Rb, Th, U, and Y were analyzed with a VG Elemental PQII Plus inductively coupled plasma mass spectrometer using the method given by Jarvis (1988). The analytical precision for major and trace elements is better than 5%. The US Geological Survey standard MAG-1 was used for calibration. Three analyses were made for each sample and averaged. For REE discussion, the chondrite normalization factors listed by McDonough and Sun (1995) were used.

Using UDASYS software (Verma et al., 2013a), we applied the analysis of variance (ANOVA) test at the 99% confidence level for the compositional data to statistically

identify the similarities between the SN and SC sands. This software uses precise and accurate critical values of F (Cruz-Huicochea and Verma, 2013) and t (Verma and Cruz-Huicochea, 2013) for the application of significance tests (F, t, and ANOVA; Verma, 2005). The samples were differentiated as 4 independent groups for ANOVA, i.e.

Gr1 and Gr2 for the medium- and fine-grained SN sands and Gr3 and Gr4 for the medium- and fine-grained SC sands, respectively, and the results are shown in Table 1. A database for source rock geochemistry was constructed from numerous references (Figure 1) and was used for comparison.

Table 1. Results of successive application of ANOVA at 99% confidence level to element concentration data for beach sands along the Gulf of California, Mexico, after separating normally distributed data based on DODESSYS (Verma and Díaz-González, 2012).

Element (% or $\mu g\ g^{-1}$)	Total no. of groups	ν_1	ν_2	F_{calc}	F_{crit}	H_0	Regions without significant differences	Regions with significant differences
SiO_2	4	3	36	408.09499	5.06516	F		Gr1, Gr2, Gr3, Gr4
Al_2O_3	4	3	36	67.79245	5.06516	F		Gr1, Gr2, Gr3, Gr4
Fe_2O_3	4	3	36	58.90667	5.06516	F		Gr1, Gr2, Gr3, Gr4
CaO	4	3	36	400.37455	5.06516	F		Gr1, Gr2, Gr3, Gr4
MgO	4	2	27	5.50142	6.48949	T	Gr1, Gr4, Gr3	Gr2
K_2O	4	3	36	972.90872	5.06516	F		Gr1, Gr2, Gr3, Gr4
Na_2O	4	3	36	61.06181	5.06516	F		Gr1, Gr2, Gr3, Gr4
TiO_2	4	3	36	147.25201	5.06516	F		Gr1, Gr2, Gr3, Gr4
P_2O_5	4	2	27	0.21952	6.48949	T	Gr2, Gr1, Gr3	Gr4
CIA	4	3	36	394.33402	5.06516	F		Gr1, Gr2, Gr3, Gr4
ICV	4	3	36	144.14957	5.06516	F		Gr1, Gr2, Gr3, Gr4
Ba	4	3	36	915.81210	5.06516	F		Gr1, Gr2, Gr3, Gr4
Co	4	3	36	163.45854	5.06516	F		Gr1, Gr2, Gr3, Gr4
Cr	4	3	36	114.28525	5.06516	F		Gr1, Gr2, Gr3, Gr4
Ni	4	3	36	17.69748	5.06516	F		Gr1, Gr2, Gr3, Gr4
Zr	4	3	36	53.60950	5.06516	F		Gr1, Gr2, Gr3, Gr4
Hf	4	3	36	47.29992	5.06516	F		Gr1, Gr2, Gr3, Gr4
Rb	4	3	36	956.40453	5.06516	F		Gr1, Gr2, Gr3, Gr4
Sc	4	3	36	24.35231	5.06516	F		Gr1, Gr2, Gr3, Gr4
Sr	4	3	36	328.53406	5.06516	F		Gr1, Gr2, Gr3, Gr4
Yb	4	3	36	61.62930	5.06516	F		Gr1, Gr2, Gr3, Gr4
K_2O/Al_2O_3	4	3	36	1015.33435	5.06516	F		Gr1, Gr2, Gr3, Gr4
Rb/Al_2O_3	4	3	36	912.46811	5.06516	F		Gr1, Gr2, Gr3, Gr4
SiO_2/Al_2O_3	4	3	36	366.75615	5.06516	F		Gr1, Gr2, Gr3, Gr4
Zr/Sc	4	3	36	54.32589	5.06516	F		Gr1, Gr2, Gr3, Gr4
Rb/Sr	4	3	36	367.06952	5.06516	F		Gr1, Gr2, Gr3, Gr4
La/Co	4	3	36	86.34060	5.06516	F		Gr1, Gr2, Gr3, Gr4
Th/Co	4	3	36	84.19590	5.06516	F		Gr1, Gr2, Th3, Gr4
Th/U	4	3	36	79.58799	5.06516	F		Gr1, Gr2, Gr3, Gr4
TREE	4	3	36	59.95990	5.06516	F		Gr1, Gr2, Gr3, Gr4
Eu/Eu^*	4	3	36	54.74642	5.06516	F		Gr1, Gr2, Gr3, Gr4

Gr1 = San Nicolás beach (medium-grained sands); Gr2 = San Nicolás beach (fine-grained sands); Gr3 = San Carlos beach (medium-grained sands); Gr4 = San Carlos beach (fine-grained sands); F = false; T = true. Subscript $_{cn}$ refers to chondrite-normalized values (McDonough and Sun, 1995). UDASYS software (Verma et al., 2013) was used for this application.

4. Results

4.1. Texture and modal analysis

The mean grain size (M_z) ranges from ~1.26 to 2.84 ⌀ for the SN sands, indicating that the sand grains are medium to fine in size (Table 2). The mean grain size for SC sands also varies from medium (1.27 ⌀) to fine (2.91 ⌀). The standard deviation values vary from ~0.53 to 0.71 ⌀ (moderately well sorted) and ~0.36 to 0.48 ⌀ (well sorted) for the medium- and fine-grained SN sands, respectively. However, the SC sands vary from poorly sorted (1.34 ⌀) to moderately sorted (0.75 ⌀) and sorting is irrespective of mean grain size (Table 2).

The average Q-F-L ratios are Q_{88}-F_4-L_8 and Q_{81}-F_5-L_{14} for the SN and SC sands, respectively (Table 3; Figure 2a). Lithic fragments are dominated by a mix of plutonic, volcanic, and sedimentary rock fragments, suggesting granite, basaltic andesite, and sandstone sources. Similarly, both SN and SC sands are composed of rock-forming minerals such as plagioclase, potash feldspar, and pyroxene. SN sands are compositionally more mature than SC sands, because more heavy minerals like rutile, zircon, and magnetite were identified in SN sands. These minerals may derive from felsic plutonic and sedimentary rocks exposed along the western side of the Gulf of California (Ramos-Velázquez et al., 2008; Roldán-Quintana et al., 2009) or from the nearby Sonora Desert (Carriquiry and Sánchez, 1999). This is supported by the fact that identified magnetite grains are homogeneous and without any intergrowth of hematite–rutile associations (Grisby, 1990).

Cluster analysis reveals that SC sands are dominant in the left-hand side and SN sands in the right-hand side of the dendrogram (Figure 2b). This result is consistent with the Q-F-L ternary diagram (Figure 2a); according to it, the SC sands were influenced by a mixture of volcanic and sedimentary lithic fragments. In contrast, the SN sands were influenced by granitic rocks, derived from the Laramide batholith exposed along the Gulf of California (Roldán-Quintana et al., 2009).

4.2. Mineralogy

The XRD study shows that the SN sands have a high proportion of quartz grains (Figure 3). Among heavy minerals, rutile is identified in the fine-grained SN sands (Figure 3a). A magnesium-rich mineral, forsterite, is identified in sample SN2 (Figure 3b). Similarly, a calcium-rich mineral is identified in the medium-grained SC sand (Figure 3c). The chemical composition of a sand grain measured using the SEM-EDS method reveals that the fine-grained SN sands are rich in a Ti-bearing mineral, probably rutile (Figure 4a). In addition, a sand grain from sample SN2 is enriched in Zr content (Figure 4b), which may be a zircon grain. Fine-grained sands from SN and SC were generally enriched in Fe content (Figure 4c). However, medium-grained SC sands were enriched in calcium (sample SC9; Figure 4d).

4.3. Major element geochemistry

The major element compositions of SN and SC beach sands are provided in Table 2. $(SiO_2)_{adj}$ content in the medium-grained SN sands (ca. 69–74 wt.%) is higher than that in the medium- and fine-grained SC sands (ca. 55–58 wt.% and 57–62 wt.%, respectively; Table 2). The application of ANOVA at the 99% confidence level reveals a significant difference in $(SiO_2)_{adj}$ content among them ($F_{calc} = 408.0950$ and $(F_{crit})_{99\%} = 5.0652$, where $F_{calc} > (F_{crit})_{99\%}$ indicates that data populations are significantly different at 99% confidence level; Table 1). The fine-grained SN and SC sands are slightly higher in Al_2O_3 content (ca. 12.07–12.64 and 10.40–11.90, respectively) than the medium-grained SN and SC sands (ca. 8.98–10.81 and 9.30–9.80, respectively) ($F_{calc} = 67.7925 > (F_{crit})_{99\%} = 5.0652$; Table 1). The MgO and P_2O_5 contents are similar for the medium-grained SN and SC sands. However, MgO is slightly enriched in the fine-grained SN sands and P_2O_5 in the fine-grained SC sands, which is also confirmed by ANOVA (Table 1). The enrichment of MgO content is probably due to the concentration of forsterite, identified by XRD (Figure 3b). Similarly, the concentration of anorthite increases the calcium content in SC sands (medium-grained sand SC9; Figure 3c). The variation in other major elements like Fe_2O_3, K_2O, Na_2O, and TiO_2 among medium- and fine-grained SN, and SC sands is significantly different at the 99% confidence level (Table 1).

We note that the use of the linear correlation coefficient (r) for compositional data should be viewed with caution (Aitchison, 1986; Verma, 2012). Nevertheless, the correlation between SiO_2 and Al_2O_3 is statistically significant at the 99% confidence level for SN (r = 0.79, number of samples n = 20) and SC (r = 0.88, n = 20; critical t value for 99% confidence level is 0.537; Verma, 2005) sands, indicating that much of SiO_2 is not present as quartz grains (Ahmad and Chandra, 2013). Similarly, a statistically significant positive correlation between Fe_2O_3 and TiO_2 for all sands (r = 0.93, n = 40; critical t value for 99% confidence level is 0.393; Verma, 2005) reveals the abundance of Fe- and Ti-bearing minerals. This observation is consistent with the results obtained by the SEM-EDS method (Figures 4a and 4c).

4.4. Trace element geochemistry

The trace element data are provided in Table 4. In comparison with the upper continental crust (UCC) (Figure 5), the sands are depleted in high field strength elements like Y, Zr, Nb, and Hf. However, the fine-grained SN sands are more enriched in Zr and Hf than the medium-grained sands, which is probably due to the abundance of the heavy mineral zircon in this fraction. The positive correlations between Zr and Hf (r = 0.99, n = 10), TiO_2 (r = 0.84, n = 10), and Fe_2O_3 (r = 0.95, n = 10; critical t value for 99% confidence level is 0.708) for the fine-grained SN

Table 2. Major element data (wt.%) of beach sands along the Gulf of California, Mexico.

Elements	San Nicolás							
	SN1		SN2		SN3		SN4	
	m	f	m	f	m	f	m	f
Mz	1.26	2.26	1.75	2.45	1.74	2.60	1.50	2.78
S	0.71	0.36	0.68	0.38	0.65	0.42	0.58	0.41
$(SiO_2)_{adj}$	69.3	73.1	73.1	72.7	72.3	73.2	68.8	72.7
SiO_2	63.7	70.9	69.3	69.9	67.6	70.3	63.1	69.7
TiO_2	0.12	0.26	0.14	0.38	0.11	0.26	0.11	0.24
Al_2O_3	10	12.4	10.8	12.3	10	12.3	9	12.4
$Fe_2O_3^*$	1.03	1.58	1.04	2.09	0.88	1.61	0.93	1.56
MnO	0.02	0.01	0.02	0.03	0.02	0.02	0.02	0.02
MgO	1.02	1.33	0.87	1.18	0.78	1.10	0.94	1.11
CaO	8.83	3.27	5.37	3.25	7.07	3.09	11.1	3.43
Na_2O	2.75	3.49	3.00	3.44	2.60	3.56	2.43	3.53
K_2O	4.15	3.65	4.20	3.49	4.22	3.74	4.01	3.77
P_2O_5	0.13	0.12	0.12	0.14	0.12	0.12	0.13	0.12
LOI	8.02	2.64	4.81	2.59	6.17	2.74	8.04	2.99
Total	99.8	99.7	99.7	98.7	99.7	98.9	99.9	98.8
CIA	42.7	44.5	42.8	44.8	43.4	43.9	42.1	44.1
ICV	1.77	1.1	1.36	1.13	1.56	1.08	2.18	1.1
SiO_2/Al_2O_3	6.31	5.72	6.44	5.7	6.73	5.71	7.03	5.63
Elements	San Nicolás							
	SN5		SN7		SN8		SN9	
	m	f	m	f	m	f	m	f
Mz	1.45	2.72	1.53	2.64	1.32	2.84	1.29	2.76
S	0.67	0.48	0.54	0.39	0.56	0.37	0.53	0.43
$(SiO_2)_{adj}$	73.3	73.0	72.3	73.2	73.7	72.8	74	73.2
SiO_2	68.9	70.2	67.3	70.6	69.9	69.5	69.9	70.1
TiO_2	0.12	0.3	0.1	0.26	0.13	0.28	0.12	0.27
Al_2O_3	10.2	12.3	9.7	12.4	10.8	12.1	10.5	12.2
$Fe_2O_3^*$	0.92	1.76	0.85	1.6	1.0	1.63	0.96	1.6
MnO	0.01	0.03	0.02	0.02	0.01	0.02	0.01	0.02
MgO	0.77	1.1	0.79	1.1	0.82	1.23	0.8	1.1
CaO	6.17	3.13	7.41	3.18	4.93	3.36	4.91	3.12
Na_2O	2.64	3.57	2.5	3.55	2.92	3.58	2.89	3.54
K_2O	4.16	3.63	4.28	3.72	4.22	3.63	4.25	3.67
P_2O_5	0.12	0.12	0.13	0.12	0.11	0.12	0.12	0.12
LOI	5.55	2.61	6.57	2.83	4.51	2.93	4.98	2.89
Total	99.6	98.7	99.7	99.3	99.3	98.4	99.4	98.7
CIA	43.6	43.9	43.1	44	43.3	43.5	42.6	43.9
ICV	1.45	1.1	1.64	1.09	1.29	1.14	1.33	1.09
SiO_2/Al_2O_3	6.75	5.72	6.93	5.71	6.46	5.76	6.69	5.74

Table 2. (Continued).

Elements	San Nicolás									
	SN10		SN11		Medium sand			Fine sand		
	m	f	m	f	n	mean	std	n	mean	std
Mz	1.48	2.58	1.68	2.54	10	1.5	0.18	10	2.62	0.17
S	0.63	0.36	0.66	0.45	10	0.62	0.06	10	0.45	0.04
$(SiO_2)_{adj}$	71.7	72.8	73.2	72.6	10	72.2	1.79	10	72.2	0.23
SiO_2	65.8	69.8	67.9	70	10	67.4	2.44	10	70.1	0.43
TiO_2	0.11	0.32	0.11	0.29	10	0.12	0.01	10	0.29	0.04
Al_2O_3	9.86	12.5	9.86	12.6	10	10.1	0.54	10	12.4	0.15
$Fe_2O_3^*$	0.97	1.67	0.91	1.69	10	0.95	0.06	10	1.68	0.15
MnO	0.02	0.02	0.02	0.02	10	0.02	0.003	10	0.021	0.004
MgO	0.82	1.13	0.84	1.12	10	0.84	0.08	10	1.15	0.07
CaO	7.11	3.14	6.21	3.31	10	6.91	1.92	10	3.23	0.11
Na_2O	2.87	3.54	2.63	3.56	10	2.72	0.19	10	3.53	0.04
K_2O	4.12	3.73	4.19	3.72	10	4.18	0.07	10	3.67	0.08
P_2O_5	0.12	0.12	0.12	0.12	10	0.12	0.01	10	0.12	0.01
LOI	8.01	3.2	6.7	2.96	10	6.34	1.37	10	2.84	0.2
Total	99.9	99.1	99.5	99.5	10	99.6	0.18	10	99	0.4
CIA	41.5	44.3	42.8	44.5	10	42.8	0.63	10	44.1	0.4
ICV	1.62	1.09	1.51	1.08	10	1.57	0.26	10	1.10	0.02
SiO_2/Al_2O_3	6.68	5.60	6.89	5.54	10	6.69	0.23	10	5.68	0.07

Elements	San Carlos							
	SC1		SC2		SC3		SC4	
	m	f	m	f	m	f	m	f
Mz	1.28	2.61	1.38	2.58	1.27	2.82	1.57	2.91
S	1.34	0.75	0.97	0.78	0.88	0.82	1.10	0.87
$(SiO_2)_{adj}$	55.1	57.3	56.6	62.3	57.2	58.8	56.5	56.6
SiO_2	44.4	49.3	46.6	53.8	47	50.9	46.3	48.3
TiO_2	0.1	0.2	0.1	0.21	0.1	0.2	0.1	0.2
Al_2O_3	9.3	10.9	9.5	11.7	9.5	11.2	9.7	10.4
$Fe_2O_3^*$	0.9	1.2	0.9	0.8	0.8	1.1	0.9	1.4
MnO	0.01	0.01	0.02	0.01	0.01	0.01	0.02	0.01
MgO	0.8	0.9	0.8	0.8	0.9	0.8	0.8	0.8
CaO	21.2	18.6	20.4	13.8	19.7	17.5	20.0	19.8
Na_2O	2.5	2.9	2.7	2.8	2.7	2.7	2.6	2.5
K_2O	1.2	1.8	1.2	2.3	1.4	2	1.4	1.8
P_2O_5	0.2	0.2	0.1	0.2	0.1	0.2	0.1	0.2
LOI	18.3	14	17.5	13.1	17.3	13.6	16.9	14.5
Total	98.9	100	99.8	99.5	99.5	100	98.8	99.9
CIA	49.4	48.7	48.3	50	47.7	50.3	49.1	50.5
ICV	2.87	2.35	2.75	1.77	2.69	2.17	2.66	2.55
SiO_2/Al_2O_3	4.77	4.52	4.91	4.60	4.95	4.55	4.77	4.64

Table 2. (Continued).

Elements	San Carlos							
	SC5		SC6		SC7		SC8	
	m	f	m	F	m	f	m	f
Mz	1.82	2.38	1.77	2.65	1.74	2.65	1.82	2.77
S	1.02	0.79	0.98	0.97	1.00	0.94	1.24	0.92
$(SiO_2)_{adj}$	58.2	59.8	57.1	59.6	58.4	59.7	56.5	58.1
SiO_2	48.1	51.9	47.3	51.4	47.8	51.6	46.5	49.2
TiO_2	0.1	0.2	0.1	0.2	0.09	0.19	0.1	0.2
Al_2O_3	9.7	10.8	9.8	10.6	9.6	10.8	9.8	10.7
$Fe_2O_3^*$	0.8	1.2	0.9	1.1	0.85	1.15	0.95	1.25
MnO	0.01	0.01	0.02	0.01	0.01	0.02	0.01	0.02
MgO	0.8	0.8	0.8	0.8	0.85	0.8	0.85	0.8
CaO	18.9	17.2	19.8	17.6	18.5	17.3	19.9	17.9
Na_2O	2.6	2.6	2.7	2.5	2.7	2.6	2.7	2.6
K_2O	1.5	1.9	1.4	1.9	1.4	1.9	1.4	1.9
P_2O_5	0.1	0.2	0.1	0.2	0.1	0.2	0.1	0.2
LOI	16.4	13	16.8	13.3	17.5	13.6	16.7	15
Total	99	99.8	99.7	99.8	99.3	99.9	99	99.6
CIA	48.8	50.4	48.5	50.8	48.5	50.8	49	50.8
ICV	2.55	2.21	2.62	2.27	2.54	2.22	2.64	2.29
SiO_2/Al_2O_3	4.94	4.81	4.83	4.85	4.97	4.8	4.75	4.59

| Elements	San Carlos				Statistical parameters					
	SC9		SC10		Medium sand			Fine sand		
	m	f	m	f	n	mean	std	n	mean	std
Mz	1.57	2.82	1.45	2.43	10	1.57	0.23	10	2.66	0.17
S	0.98	0.86	1.21	0.77	10	1.07	0.15	10	0.85	0.08
$(SiO_2)_{adj}$	56.6	60.1	58.4	58.7	10	57.1	1.05	10	59.1	1.6
SiO_2	45.7	51.5	48.6	50.1	10	46.8	1.2	10	50.8	1.6
TiO_2	0.1	0.2	0.1	0.1	10	0.10	0.003	10	0.20	0.01
Al_2O_3	9.4	11.9	9.6	11.1	10	9.6	0.17	10	11	0.48
$Fe_2O_3^*$	0.9	0.9	0.82	1.03	10	0.87	0.05	10	1.11	0.17
MnO	0.01	0.02	0.02	0.02	10	0.01	0.005	10	0.01	0.005
MgO	0.8	0.8	0.83	0.9	10	0.82	0.03	10	0.82	0.04
CaO	19.9	15.2	19	17.4	10	19.7	0.77	10	17.2	1.66
Na_2O	2.65	2.7	2.62	2.8	10	2.64	0.06	10	2.66	0.14
K_2O	1.25	2.2	1.51	1.7	10	1.36	0.11	10	1.93	0.19
P_2O_5	0.1	0.2	0.1	0.2	10	0.11	0.03	10	0.2	0.0
LOI	18.8	14.1	16.7	14.4	10	17.3	0.8	10	13.8	0.65
Total	99.7	99.7	99.9	99.7	10	99.4	0.41	10	99.8	0.2
CIA	48.3	51.4	48.4	50	10	48.6	0.48	10	50.4	0.72
ICV	2.73	1.85	2.59	2.17	10	2.66	0.1	10	2.18	0.23
SiO_2/Al_2O_3	4.86	4.34	5.07	4.54	10	4.88	0.1	10	4.62	0.16

m = Medium sand; f = fine sand; n = number of samples; std = standard deviation; Mz = mean grain size (in ϕ units); S = standard deviation (in ϕ units); $(SiO_2)_{adj}$ = major element data were recalculated to anhydrous (LOI-free) basis and adjusted to 100%; $Fe_2O_3^*$ = total Fe expressed as Fe_2O_3. CIA = $[Al_2O_3/(Al_2O_3 + CaO^* + Na_2O + K_2O)] \times 100$ (Nesbitt and Young, 1982). CaO^* = CaO in silicate phase. To calculate CaO^* the assumption proposed by McLennan et al. (1993) was followed. ICV = $(Fe_2O_3 + K_2O + Na_2O + CaO + MgO + MnO + TiO_2)/Al_2O_3$ (Cox et al., 1995).

Table 3. Modal analysis data for beach sands along the Gulf of California.

| Beach	San Nicolás						San Carlos					
Sample #	SN1	SN2	SN3	SN4	SN7	SN8	SC1	SC7	SC7	SC8	SC8	SC10
	m	m	m	m	f	m	f	m	f	m	f	m
Q	241	225	232	213	253	251	243	196	203	178	190	244
K	8	5	2	3	2	4	3	1	1	4	1	5
P	5	4	10	7	8	5	10	11	12	11	10	9
Lv	12	9	14	11	11	13	21	20	12	14	12	15
Ls	17	9	7	9	6	6	22	19	14	27	22	20
Lm	2	1	0	0	0	0	0	0	0	0	0	0
HM	15	39	17	5	19	15	1	0	0	0	0	7
B	0	8	18	52	1	6	0	53	58	66	65	0
n	300	300	300	300	300	300	300	300	300	300	300	300

Grain parameters: Q = total quartz, K = potash feldspar, P = plagioclase, Lv = volcanic lithic fragments, Ls = sedimentary lithic fragments, Lm = metamorphic lithic fragments, HM = heavy minerals, B = biogenic components (shell, algae, and coral), n = number of grains counted, m = medium-grained sand; f = fine-grained sand.
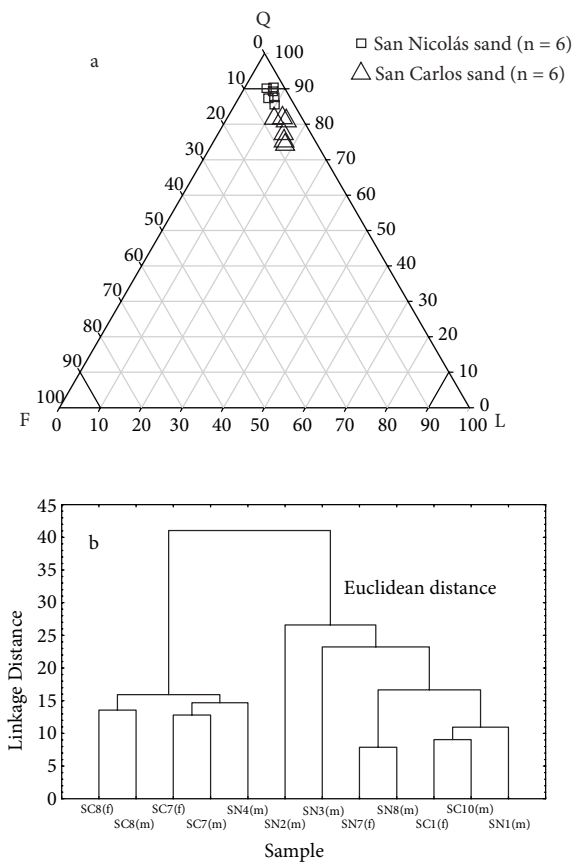
Figure 2. a) Q-F-L (Dickinson et al., 1983) triangular diagram. Q = total quartz, F = total feldspar [K (potash feldspar) + P (plagioclase)], and L = total lithic fragments [volcanic (Lv) + sedimentary (Ls) + metamorphic (Lm) + plutonic (Lp)]. **b)** Dendrogram for the modal data (refer to Table 3 for data).
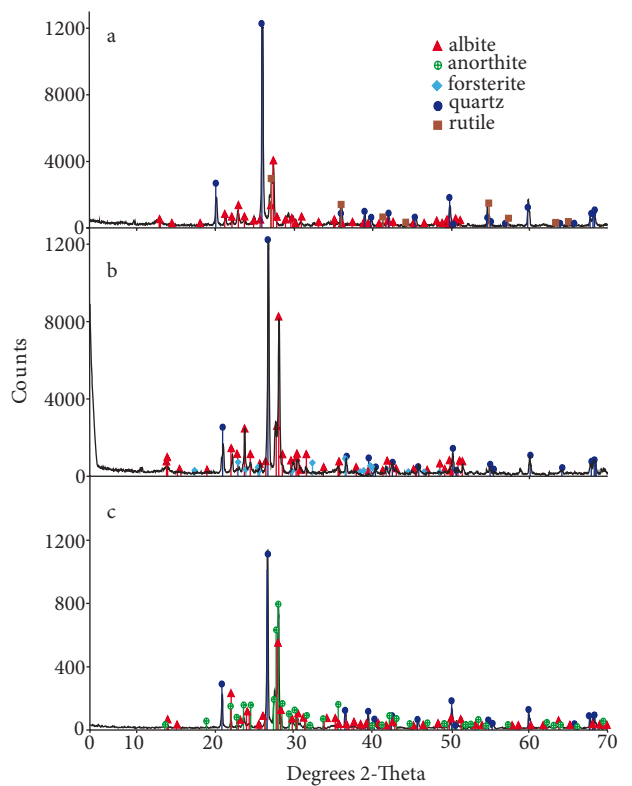
Figure 3. X-ray diffraction patterns of the beach sand samples: **a)** San Nicolás (sample SN1); **b)** sample no. SN2; **c)** San Carlos medium-grained sand SC9.
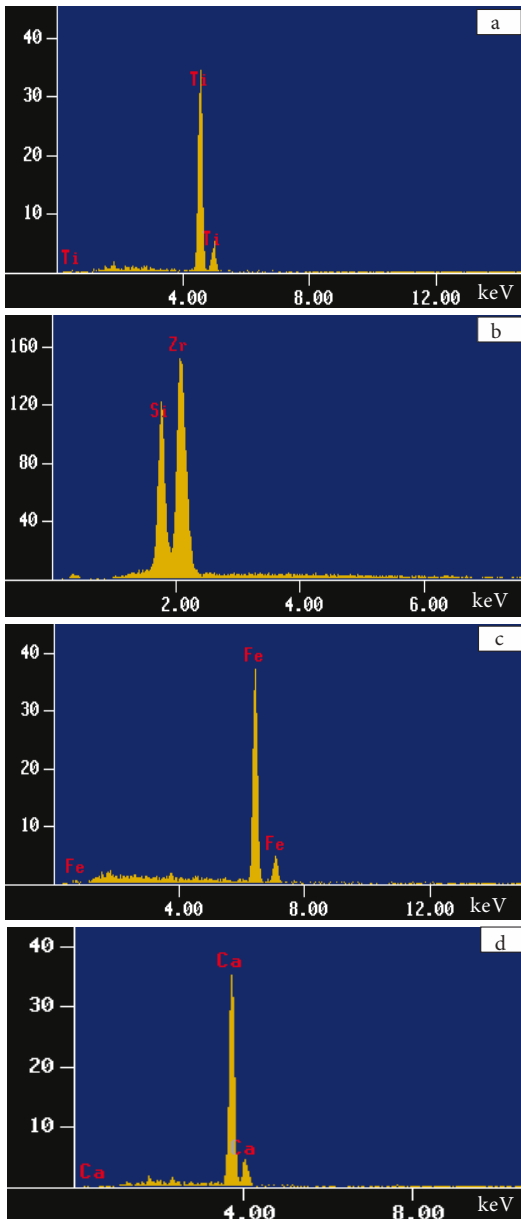
Figure 4. SEM and EDS spectra for the beach sand samples. **a)** Sample no. SN1; **b)** sample SN2; **c)** sample SN5; **d)** sample SC9.

sands indicates that these elements are probably hosted by accessory minerals like zircon, rutile, and magnetite. The SEM-EDS study also reveals the enrichment of Ti, Zr, and Fe contents among the fine-grained SN sands (Figures 4a–4c).

The concentrations of large ion lithophile elements such as Rb and Ba are higher in SN than in SC sands (Tables 1 and 4). The correlation between Rb and Ba is statistically significant at the 99% confidence level for the medium-grained (r = 0.71, n = 10) and fine-grained (r = 0.89, n = 10; critical t value for 99% confidence level is 0.708) SC sands.

However, this correlation is not statistically significant for the medium-grained (r = 0.33, n = 10) and fine-grained (r = 0.33, n = 10) SN sands. In addition, Rb and Ba are correlated statistically significant with K_2O for the fine- and medium-grained SN and SC sands, suggesting that the distribution of these elements may be controlled by alkali feldspar. The difference in the Sr content among the medium- and fine-grained SN, and SC sands is statistically significant (F_{calc} = 328.5340546 > $(F_{crit})_{99\%}$ = 5.065158; Table 1) and it is enriched in the medium- and fine-grained SC sands. Similarly, the transition trace elements like V, Cr, Co, Cu, Ni, and Sc are concentrated more in the fine-grained sands than in the medium-grained sands (Figure 5). The correlation between Al_2O_3 and Co (r = 0.95, n = 20), Ni (r = 0.70, n = 20), and Sc (r = 0.94, n = 20) is statistically significant for the SN sands, whereas it is not statistically significant for the SC sands (r = 0.18, 0.04, and 0.35, respectively, n = 20; critical t value for 99% confidence level is 0.537; Verma, 2005). The statistically significant positive correlation obtained for the SN sands suggests that in the SN sands elements such as Co, Ni, and Sc are mainly associated in clay minerals.

4.5. Rare earth element geochemistry
The REE data are given in Table 5 and are shown as chondrite-normalized patterns in Figure 6. The ΣREE contents vary widely between the 2 beach areas. The fine-grained SN and SC sands are higher in ΣREE content than the medium-grained sands (F_{calc} = 59.9599001 > $(F_{crit})_{99\%}$ = 5.065158; Table 1). The chondrite-normalized REE patterns for the SC sands show fractionated light rare earth elements (LREEs) and depleted heavy rare earth elements (HREEs) with little variation in the size of the Eu anomaly. The depletion of HREEs in the SC sands may be due to the low concentration of zircon, which normally increases the HREE content in sediments (Nardi et al., 2013). The chondrite-normalized REE patterns for the SN sands appear similar to the UCC with flat LREEs and enriched HREEs, characterized by a negative Eu anomaly. A small enrichment of HREEs in SN sands can be attributed to the abundance of phases that retain HREEs (e.g., zircon). A statistically significant positive correlation for Zr content with Yb (r = 0.90, n = 10) and HREEs (r = 0.62, n = 10; critical t value for 99% confidence level is 0.708; Verma, 2005) for the fine-grained SN sands suggests that these elements are probably hosted by accessory mineral zircon.

The correlation between ΣREE and Al_2O_3 for the fine-grained SN sands is not statistically significant (r = –0.13, n = 10), which suggests that REEs are mainly housed in heavy minerals rather than in clay minerals. A statistically significant positive correlation observed between ΣREE and TiO_2 (r = 0.92, n = 10), Fe_2O_3 (r = 0.98, n = 10), and P_2O_5 (r = 0.93, n = 10; critical t value for 99% confidence level is 0.708) contents for the fine-grained SN sands also

Table 4. Trace element concentration (ppm) of beach sands along the Gulf of California, Mexico.

| Elements | San Nicolás | | | | | | | |
| | SN1 | | SN2 | | SN3 | | SN4 | |
	m	f	m	f	m	f	m	f
Ba	883	860	939	850	948	852	883	866
Co	2.2	3.7	2.2	4.2	1.7	3.7	1.8	3.6
Cr	7.2	15	7.6	19	6	14	5.4	13
Cs	3	3.3	2.9	3.3	2.7	3.3	2.7	3.4
Cu	-	-	-	-	-	-	-	-
Ga	-	-	-	-	-	-	-	-
Hf	1.8	2.2	1.9	5.5	1.6	2.8	1.5	2.4
Nb	-	-	-	-	-	-	-	-
Ni	6.1	8.8	4.3	14	5.7	7.1	4.5	5.9
Pb	-	-	-	-	-	-	-	-
Rb	131	115	133	118	133	124	127	128
Sc	1.7	3.5	1.8	4.4	1.4	3.4	1.4	3.1
Sr	535	332	414	359	446	330	628	362
Th	5.1	6.2	5.1	7.6	4.8	6.1	4.9	6.1
U	1.7	1.9	1.6	2.7	1.6	1.8	1.7	2.0
V	-	-	-	-	-	-	-	-
Y	-	-	-	-	-	-	-	-
Zn	21	29	20	32	18	28	17	28
Zr	65	77	61	210	66	100	59	93
Th/U	3	3.3	3.1	2.9	3	3.4	2.9	3.1
Zr/Sc	38	22	34	48	47	29	42	30
La/Sc	9	5.4	8.4	5.8	10	5.8	11	5.9
Th/Sc	3	1.8	2.8	1.7	3.4	1.8	3.5	2
La/Co	7	5.1	6.9	6	8.2	5.3	8.2	5.1
Th/Co	2.3	1.7	2.3	1.8	2.9	1.7	2.7	1.7
Cr/Th	1.4	2.4	1.5	2.5	1.2	2.3	1.1	2.1
Elements	San Nicolás							
	SN5		SN7		SN8		SN9	
	m	f	m	f	m	f	m	f
Ba	932	880	924	863	923	834	922	840
Co	1.9	3.9	1.7	3.8	2	3.8	1.9	3.9
Cr	6.2	16	5.3	15	7.3	14.5	7.1	15
Cs	2.7	3.3	2.8	3.3	2.8	3.3	2.8	3.4
Cu	-	-	-	-	-	-	-	-
Ga	-	-	-	-	-	-	-	-
Hf	1.7	3.6	1.5	2.8	1.8	2.8	1.7	2.8
Nb	-	-	-	-	-	-	-	-
Ni	6.6	9.7	5	11	4.8	12	4.2	12
Pb	-	-	-	-	-	-	-	-
Rb	133	121	133	113	129	113	122	113

Table 4. (Continued).

Sc	1.5	3.6	1.3	3.4	1.6	3.5	1.5	3.5
Sr	409	331	449	362	361	317	358	322
Th	4.9	6.3	4.5	6	4.7	6	4.4	6
U	1.6	2.1	1.6	1.9	1.6	2.1	1.5	2.0
V	-	-	-	-	-	-	-	-
Y	-	-	-	-	-	-	-	-
Zn	18	30	15	29	20	29	20	30
Zr	63	145	40	102	71	109	70	110
Th/U	3.1	3.2	2.8	3.2	3.1	3.1	2.9	3.1
Zr/Sc	42	40	31	30	44	31	47	31
La/Sc	9.5	5.6	10.1	5.6	8.5	5.6	8.9	5.6
Th/Sc	3.3	1.8	3.4	1.8	2.9	1.7	2.9	1.7
La/Co	7.5	5.1	7.9	5	6.8	5.2	7.1	5
Th/Co	2.6	1.6	2.6	1.6	2.1	1.6	2.3	1.6
Cr/Th	1.3	2.5	1.2	2.4	1.6	2.4	1.6	2.4

	San Nicolás				Statistical parameters					
Elements	SN10		SN11		Medium sand			Fine sand		
	m	f	m	f	n	mean	std	n	mean	std
Ba	910	848	928	875	10	919	22	10	857	14
Co	1.9	3.5	1.8	3.7	10	1.9	0.18	10	3.9	0.19
Cr	6.3	15	5.9	15.4	10	6.4	0.83	10	15.1	1.7
Cs	2.6	3.3	2.7	3.2	10	2.8	0.12	10	3.3	0.04
Cu	-	-	-	-	-	-	-	-	-	-
Ga	-	-	-	-	-	-	-	-	-	-
Hf	1.6	2.7	1.6	3.6	10	1.7	0.1	10	3.1	0.95
Nb	-	-	-	-	-	-	-	-	-	-
Ni	5.2	6.8	6.2	9.4	10	5.3	0.85	10	9.7	2.6
Pb	-	-	-	-	-	-	-	-	-	-
Rb	128	124	128	118	10	130	3.5	10	119	5.4
Sc	1.5	3.3	1.4	3.5	10	1.5	0.15	10	3.5	0.34
Sr	421	325	401	329	10	407	161	10	305	107
Th	4.5	6.1	4.9	6.1	10	4.8	0.26	10	6.3	0.49
U	1.5	1.8	1.6	1.9	10	1.6	0.07	10	2	0.24
V	-	-	-	-	-	-	-	-	-	-
Y	-	-	-	-	-	-	-	-	-	-
Zn	18	25	18	29	10	17	1.6	10	29	1.7
Zr	65	97	61	141	10	62	8.7	10	118	38
Th/U	3.1	3.4	3.1	3.2	10	3	0.11	10	3.2	0.17
Zr/Sc	43	29	44	40	10	2.2	0.26	10	33	7.4
La/Sc	9.4	6.0	10	5.7	10	9.5	0.78	10	5.7	0.19
Th/Sc	3.0	1.8	3.5	1.8	10	3.2	0.27	10	1.8	0.08
La/Co	7.4	5.7	7.9	5.4	10	7.5	0.55	10	5.3	0.33
Th/Co	2.4	1.7	2.7	1.7	10	7.5	0.55	10	5.3	0.33
Cr/Th	1.4	2.5	1.2	2.5	10	1.3	0.2	10	2.4	0.13

Table 4. (Continued).

Elements	San Carlos SC1 m	f	SC2 m	f	SC3 m	f	SC4 m	f
Ba	405	460	395	531	422	479	427	450
Co	2.6	2.5	2.3	2.1	2.1	2.6	2.2	2.5
Cr	8.4	13	8.8	10	6.9	12.1	7.7	12
Cs	1.1	1.2	1.1	1.4	1.2	1.3	1.1	1.2
Cu	11	54	14	27	9	23	11	20
Ga	22	25	22	28	22	26	23	24
Hf	0.76	0.95	0.81	1.1	0.83	0.98	0.84	0.90
Nb	0.36	3.2	1.1	2.7	2.4	3.1	2.3	2.8
Ni	7.5	6.8	7.4	6.9	7.2	7.1	6.7	7
Pb	7.6	8.3	8.2	9.1	7.8	8.5	7.8	8.5
Rb	48	52	52	66	55	57	51	54
Sc	2.9	1.0	1.0	2.5	1.0	3.3	1.0	3.1
Sr	995	977	922	792	960	935	981	969
Th	2.8	3.5	3.3	3.6	2.4	3.9	2.3	4.2
U	1.6	1.5	1.5	1.5	1.4	1.6	1.4	1.6
V	18	24	15	16	13	21	15	26
Y	7.9	9.7	7.7	8.5	7.7	10	7.3	9.6
Zn	20	21	19	18	23	19	19	19
Zr	21	22	21	27	21	22	20	21
Th/U	1.8	2.3	2.2	2.4	1.8	2.5	1.7	2.5
Zr/Sc	7.2	22	21	10	21	6.6	20.5	6.8
La/Sc	3.4	14	10	4.2	8.6	4.1	9.2	4.7
Th/Sc	0.97	3.5	3.3	1.4	2.4	1.2	2.3	1.3
La/Co	3.8	6	4.4	5.1	4.1	5.2	4.2	5.8
Th/Co	1.1	1.4	1.4	1.7	1.2	1.5	1.0	1.7
Cr/Th	3.0	3.9	2.7	2.8	2.9	3.1	3.4	2.9

Elements	San Carlos SC5 m	f	SC6 m	f	SC7 m	f	SC8 m	f
Ba	506	481	459	459	448	448	420	450
Co	1.9	2.8	2.1	2.7	2.0	2.5	2.7	2.6
Cr	6.2	12.4	7.5	11.6	7.3	11.5	7.6	11.7
Cs	1.2	1.3	1.1	1.3	1.1	1.3	1.1	1.2
Cu	9.4	16	8.6	13	8.6	13.6	11	20
Ga	23	25	22	25	23	25	23	24
Hf	0.97	0.99	0.87	0.78	0.85	0.77	0.86	0.94
Nb	2.2	3	2.2	1.9	2.2	1.8	2.3	2.8
Ni	6.3	6.9	6.6	7.0	6.6	7.3	6.8	7.6
Pb	8.4	8.3	7.8	8.2	7.8	8.2	7.9	8.7
Rb	55	56	52	56	54	55	52	55
Sc	1.7	3.7	2.2	3.5	2.1	3.5	1.1	3.2

Table 4. (Continued).

Sr	948	946	974	924	965	918	984	972
Th	2.3	2.8	2.2	2.7	2.2	2.7	2.3	4.1
U	1.3	1.5	1.3	1.5	1.3	1.4	1.4	1.7
V	12.6	20	15	20	14.7	20	15	26
Y	7.0	9.7	7.3	9.4	7.1	9.4	7.4	9.7
Zn	16	19	16	19	16	19	19	19
Zr	25	24	20	22	20	23	20	22
Th/U	1.7	1.9	1.7	1.9	1.7	1.9	1.7	2.4
Zr/Sc	14	6.6	9.1	6.4	9.5	6.5	18	6.7
La/Sc	5	3.1	4.0	3.4	4.2	3.4	8.3	4.5
Th/Sc	1.3	0.77	0.98	0.78	1.0	0.79	2.1	1.3
La/Co	4.7	4.1	4.2	4.5	4.4	4.6	4.2	5.6
Th/Co	1.2	1.0	1.0	1.0	1.1	1.1	1.1	1.6
Cr/Th	2.7	4.4	3.5	4.2	3.4	4.2	3.3	2.9

	San Carlos				Statistical parameters					
Elements	SC9		SC10		Medium sand			Fine sand		
	m	f	m	f	n	mean	std	n	mean	std
Ba	398	495	486	455	10	437	37	10	470	26
Co	2.3	2.0	2.1	2.5	10	2.2	0.19	10	2.5	0.25
Cr	8.2	10	6.5	13.3	10	7.5	0.82	10	12	1.2
Cs	1.0	1.3	1.1	1.2	10	1.1	0.04	10	1.3	0.08
Cu	13	25	9.7	46	10	11	2	10	25	14
Ga	23	28	22	24	10	23	0.34	10	25	1.4
Hf	0.84	1.0	0.92	0.93	10	0.71	0.32	10	0.94	0.10
Nb	1.1	2.5	2.2	3.1	10	1.8	0.71	10	2.7	0.49
Ni	7.1	6.8	6.4	7	10	6.9	0.42	10	7.0	0.23
Pb	8	9	8.2	8.4	10	7.9	0.23	10	8.5	0.30
Rb	50	63	54	51	10	52	2.22	10	56	4.7
Sc	1.0	2.3	1.2	1.0	10	1.5	0.67	10	2.7	0.99
Sr	918	798	925	955	10	957	27	10	919	68
Th	3.1	3.4	3.2	3.5	10	2.6	0.45	10	3.4	0.53
U	1.4	1.5	1.3	1.5	10	1.4	0.09	10	1.5	0.07
V	15	16	14	22	10	14	1.3	10	21	3.4
Y	7.6	8.3	7.5	9.5	10	7.4	0.27	10	9.4	0.54
Zn	18	18	19	22	10	18	2.01	10	19	1.6
Zr	20	26	20	22	10	21	1.61	10	23	2.08
Th/U	2.2	2.3	2.4	2.3	10	1.9	0.28	10	2.2	0.26
Zr/Sc	20	11	16	21	10	16	5.5	10	10.5	6.2
La/Sc	10	4.6	7.1	14	10	7	2.6	10	6.1	4.4
Th/Sc	3.2	1.5	2.6	3.4	10	2.0	0.89	10	1.6	1.0
La/Co	4.4	5.3	4.3	5.7	10	4.3	0.24	10	5.2	0.63
Th/Co	1.4	1.7	1.6	1.4	10	4.3	0.24	10	5.2	0.63
Cr/Th	2.6	2.9	2.0	3.8	10	3	0.46	10	3.5	0.66

Numbers were rounded following the procedure given by Verma (2005).
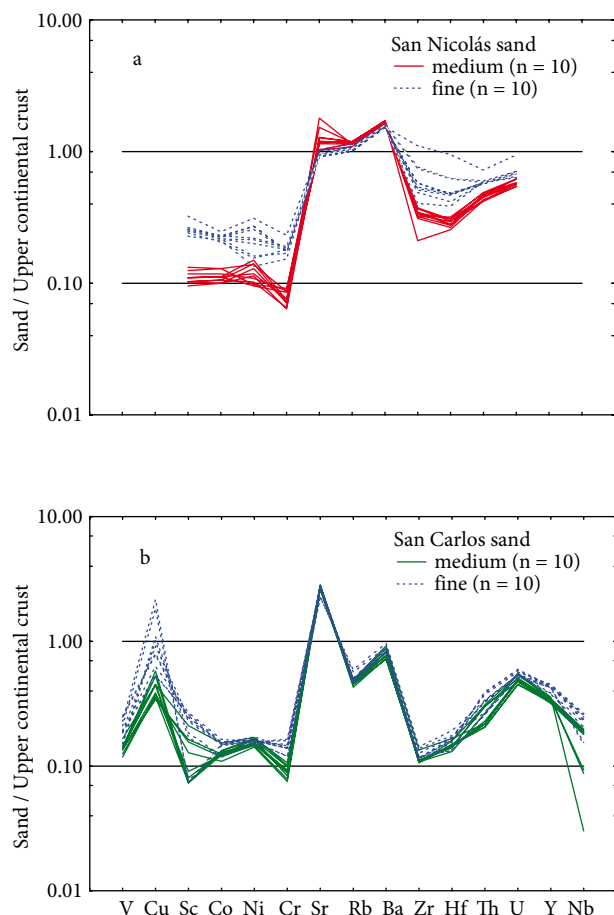
Figure 5. Multielement diagram normalized against average upper continental crust (Taylor and McLennan, 1985). A horizontal line for sand/upper continental crust value of 1 is included for reference. **a)** San Nicolás sand; **b)** San Carlos sand.

supports this observation. On the other hand, for the fine-grained SC sands the correlation for ΣREE versus TiO_2 is not statistically significant (r = –0.30, n = 10), indicating the low abundance of the Ti-bearing mineral rutile. The XRD and SEM-EDS results reveal that the fine-grained SN sands are concentrated with heavy minerals like rutile and zircon (Figures 3a and 4b, respectively).

5. Discussion

5.1. Weathering in the source area

The weathering of igneous rocks results in the removal and depletion of alkaline cations such as Na^+, K^+, and Ca^+ and the preferential enrichment of residual Al_2O_3 in the soil profile (Nesbitt and Young, 1982; Selvaraj and Chen, 2006). Hence, the weathering history of source rocks may affect the mineralogy and geochemical signatures of the terrigenous sediments. A chemical index widely used to determine the degree of source area weathering is the

chemical index of alteration (CIA; Nesbitt and Young, 1982), with higher values suggesting intense chemical weathering (Armstrong-Altrin et al., 2013; Deepthi et al., 2013; Sun et al., 2013; Zaid, 2013). This can be calculated using molecular proportions, from the formula CIA = $[Al_2O_3 / (Al_2O_3 + CaO^* + Na_2O + K_2O)] \times 100$, where CaO^* represents the amount in silicates only. In this study, CaO was corrected by following the methodology proposed by McLennan et al. (1993), in which CaO values are accepted only if CaO < Na_2O; when CaO > Na_2O, it is assumed that the concentration of CaO equals that of Na_2O. The average CIA values for the SN and SC beach sands are ~41–45 and 48–51, respectively (Table 2), and they are low relative to the range of the Post-Archaean Australian shale value (PAAS; ca. 70–75; Taylor and McLennan, 1985). The difference in the average CIA values among the SN medium- and fine-grained sands (the mean with 1 standard deviation value being 43 ± 0.63 and 44 ± 0.40, respectively) and the SC sands (49 ± 1.00) is statistically significant (F_{calc} = 394.33402 > $(F_{crit})_{99\%}$ = 5.065158; Table 1). These low CIA values in the SN and SC sands indicate low intensity of chemical weathering, which may reflect cold and/or arid climate conditions in the source area (McLennan et al., 1993).

Th/U ratios can also be used to understand the source area weathering, as the surface weathering process elevates the ratio between Th and U to above the average UCC value (Th/U = 3.8; Taylor and McLennan, 1985) due to the oxidation of U^{4+} to the more soluble U^{6+}. A Th/U ratio above 3.8 is expected to be indicative of weathering history (McLennan et al., 1993). Th/U ratios for the studied beach sands are <3.8, indicating a low degree of chemical weathering in the source area (Table 4; Figure 7). Intensive chemical weathering and diagenesis often leaches Sr compared to Rb (Nesbitt and Young, 1982). This leads to an increase of the Rb/Sr ratio and high ratios are indicators of strong weathering (McLennan et al., 1993). The Rb/Sr ratios of the SN and SC beach sands (ca. 0.203–0.328 and 0.048–0.084, respectively) are lower than the average PAAS value (0.80; Taylor and McLennan, 1985). These low Rb/Sr and Th/U ratios suggest low to moderate weathering intensity in the source area.

5.2. Hydraulic sorting

Sediment sorting is one of the important factors that define the composition of bulk sediment. It is also widely accepted that hydraulic sorting could lead to preferential enrichment of specific minerals in certain grain size fractions (Singh, 2009; Wu et al., 2013). Geochemical variability due to hydraulic sorting can be evaluated using the index of compositional variability (ICV) (Cox et al., 1995). Rock-forming minerals such as plagioclase, k-feldspars, amphiboles, and pyroxenes show ICV values of >0.84, whereas typical alteration products such as

Table 5. Rare earth element concentrations (ppm) of beach sands along the Gulf of California, Mexico.

Elements	San Nicolás							
	SN1		SN2		SN3		SN4	
	m	f	m	f	m	f	m	f
La	15.3	18.8	15.1	25.3	13.9	19.6	14.8	18.4
Ce	30.3	36.1	28.8	49	26.6	37.5	29.9	35.1
Pr	-	-	-	-	-	-	-	-
Nd	11.4	12.9	10.7	20.1	9.9	14.9	10.1	14.1
Sm	2.1	2.9	2.2	4	1.9	2.9	2.1	2.8
Eu	0.59	0.75	0.60	0.92	0.54	0.76	0.54	0.74
Gd	2	3	2	3.8	1.8	2.8	1.6	2.4
Tb	0.30	0.41	0.30	0.56	0.27	0.42	0.29	0.38
Dy	-	-	-	-	-	-	-	-
Ho	0.36	0.44	0.34	0.71	0.31	0.55	0.38	0.46
Er	-	-	-	-	-	-	-	-
Tm	0.13	0.17	0.13	0.28	0.12	0.20	0.15	0.17
Yb	0.92	1.2	0.95	1.9	0.88	1.3	0.90	1.2
Lu	0.16	0.21	0.17	0.27	0.15	0.23	0.16	0.21
LREE	59	71	57	98	52	74	56	70
HREE	3.9	5.4	3.9	7.5	3.5	5.5	3.5	4.8
TREE	63	76	61	106	56	81	60	75
Eu/Eu*	0.86	0.77	0.87	0.71	0.87	0.80	0.86	0.85

Elements	San Nicolás							
	SN5		SN7		SN8		SN9	
	m	f	m	f	m	f	m	f
La	14.2	20	13.5	19	13.6	19.6	13.4	19.6
Ce	27.3	38.7	25.8	36.2	25.2	36.7	25	36.7
Pr	-	-	-	-	-	-	-	-
Nd	10.4	15.2	10.2	13	8.9	13.4	8.7	13.4
Sm	2	3.1	1.9	2.8	2	3.1	2	3.1
Eu	0.55	0.79	0.52	0.74	0.54	0.76	0.53	0.76
Gd	1.6	2.2	1.9	2.8	1.9	2.7	1.8	2.7
Tb	0.27	0.42	0.26	0.39	0.27	0.42	0.26	0.41
Dy	-	-	-		-	-	-	-
Ho	0.38	0.51	0.34	0.54	0.34	0.54	0.34	0.54
Er	-	-	-	-	-	-	-	-
Tm	0.14	0.19	0.13	0.20	0.12	0.20	0.12	0.19
Yb	0.86	1.4	0.82	1.3	0.85	1.3	0.85	1.3
Lu	0.16	0.23	0.16	0.22	0.16	0.23	0.16	0.24
LREE	54	77	51	71	50	73	49	72
HREE	3.4	5	3.6	5.4	3.6	5.4	3.5	5.4
TREE	57	83	55	77	54	79	53	78
Eu/Eu*	0.92	0.89	0.83	0.79	0.84	0.79	0.84	0.79

Table 5. (Continued).

Elements	San Nicolás				Statistical parameters					
	SN10		SN11		Medium sand			Fine sand		
	m	f	m	f	n	mean	std	n	mean	std
La	14.1	19.8	14.3	19.8	10	14.2	0.66	10	20	1.9
Ce	26.9	37.7	27.5	38.5	10	27.3	1.8	10	38.2	4
Pr	-	-	-	-	-	-	-	-	-	-
Nd	10.1	15.1	10.5	15.0	10	10.1	0.80	10	14.7	2.1
Sm	2.1	3	2	3	10	2	0.10	10	3.1	0.33
Eu	0.55	0.77	0.56	0.77	10	0.55	0.03	10	0.78	0.05
Gd	1.8	2.9	1.6	2.0	10	1.8	0.15	10	2.7	0.49
Tb	0.28	0.45	0.28	0.40	10	0.28	0.01	10	0.43	0.05
Dy	-	-	-	-	-	-	-	-	-	-
Ho	0.32	0.54	0.39	0.49	10	0.35	0.03	10	0.53	0.07
Er	-	-	-	-	-	-	-	-	-	-
Tm	0.12	0.19	0.15	0.18	10	0.13	0.01	10	0.20	0.03
Yb	0.91	1.4	0.89	1.3	10	0.88	0.04	10	1.4	0.21
Lu	0.16	0.24	0.16	0.21	10	0.16	0.01	10	0.23	0.02
LREE	53	76	54	76	10	54	3.2	10	76	8.2
HREE	3.6	5.6	3.54	4.6	10	3.6	0.16	10	5.5	0.81
TREE	57	82	58	82	10	57	3.3	10	82	9
Eu/Eu*	0.84	0.80	0.92	0.90	10	0.83	0.03	10	0.81	0.06

Elements	San Carlos							
	SC1		SC2		SC3		SC4	
	m	f	m	f	m	f	m	f
La	9.7	14.8	10	10	8.6	13.7	9.2	14.8
Ce	18.4	28.1	18.2	19.3	16.0	26	17	27.3
Pr	2.2	3.1	2.1	2.3	1.9	2.9	2	3
Nd	11.2	16	10.9	11.7	9.7	15.4	10.3	15.9
Sm	1.8	2.3	1.7	1.9	1.6	2.3	1.7	2.5
Eu	0.61	0.74	0.61	0.71	0.58	0.77	0.62	0.73
Gd	1.9	2.5	1.9	2.0	1.7	2.5	1.8	2.4
Tb	0.23	0.30	0.22	0.25	0.21	0.31	0.21	0.29
Dy	1.4	1.7	1.3	1.5	1.3	1.8	1.3	1.9
Ho	0.26	0.33	0.26	0.29	0.25	0.35	0.25	0.34
Er	0.79	0.99	0.79	0.88	0.76	1.1	0.76	1.1
Tm	0.10	0.13	0.11	0.12	0.10	0.14	0.10	0.13
Yb	0.79	0.96	0.76	0.86	0.75	0.98	0.73	0.91
Lu	0.11	0.14	0.11	0.13	0.11	0.14	0.11	0.14
LREE	43	64	43	46	38	60	40	63
HREE	5.6	7	5.4	6	5.2	7.3	5.2	6.9
TREE	49	72	48.9	52.4	43.6	68.4	46	70.9
Eu/Eu*	0.99	0.94	1.0	1.1	1.1	0.97	1.1	0.95

Table 5. (Continued).

Elements	San Carlos							
	SC5		SC6		SC7		SC8	
	m	f	m	f	m	f	m	f
La	8.7	11.4	8.9	11.9	8.9	11.6	9.1	14.6
Ce	15.7	21.9	16.2	22.6	16	22	16.1	27.2
Pr	1.8	2.6	2	2.6	2	2.6	2	3
Nd	9.5	13.4	9.8	13.6	9.7	13.4	10.3	15.7
Sm	1.5	2.2	1.7	2.2	1.6	2.2	1.7	2.2
Eu	0.58	0.74	0.68	0.74	0.63	0.74	0.61	0.72
Gd	1.6	2.4	1.7	2.3	1.7	2.3	1.8	2.3
Tb	0.20	0.30	0.26	0.28	0.22	0.28	0.21	0.28
Dy	1.2	1.7	1.2	1.7	1.2	1.7	1.2	1.7
Ho	0.23	0.34	0.28	0.33	0.27	0.32	0.24	0.32
Er	0.71	1.02	0.76	0.99	0.75	1.0	0.74	1.0
Tm	0.11	0.14	0.11	0.13	0.11	0.13	0.10	0.12
Yb	0.70	0.94	0.74	0.91	0.72	0.92	0.74	0.91
Lu	0.10	0.14	0.11	0.13	0.11	0.13	0.10	0.13
LREE	37	51	38	52	38	52	39	62
HREE	4.9	7	5.2	6.7	5.1	6.8	5.1	6.7
TREE	42	59	44	60	43	59	45	70
Eu/Eu*	1.1	0.99	1.2	1.0	1.2	0.99	1.1	0.96

Elements	San Carlos				Statistical parameters					
	SC9		SC10		Medium sand			Fine sand		
	m	f	m	f	n	mean	std	n	mean	std
La	10	10.6	8.8	14.5	10	9.2	0.52	10	12.8	1.8
Ce	18	19.5	15.9	27.8	10	16.8	1.1	10	24.2	3.5
Pr	2	2.5	2	3	10	2	0.09	10	2.8	0.29
Nd	10.6	11.9	9.6	15.9	10	10.1	0.59	10	14.3	1.7
Sm	1.7	2	1.6	2.2	10	1.7	0.07	10	2.2	0.14
Eu	0.60	0.73	0.59	0.73	10	0.61	0.03	10	0.73	0.01
Gd	1.8	2.1	1.7	2.3	10	1.8	0.09	10	2.3	0.16
Tb	0.21	0.26	0.20	0.28	10	0.21	0.02	10	0.28	0.02
Dy	1.3	1.6	1.2	1.6	10	1.3	0.05	10	1.7	0.08
Ho	0.25	0.31	0.24	0.32	10	0.25	0.02	10	0.32	0.02
Er	0.78	0.98	0.70	0.97	10	0.75	0.03	10	0.99	0.05
Tm	0.10	0.13	0.10	0.13	10	0.10	0.003	10	0.13	0.01
Yb	0.75	0.88	0.70	0.90	10	0.74	0.03	10	0.92	0.04
Lu	0.11	0.13	0.10	0.14	10	0.11	0.01	10	0.14	0.01
LREE	42	46	37	63	10	39	2.3	10	56	7.4
HREE	5.3	6.4	4.9	6.6	10	5.2	0.21	10	6.7	0.36
TREE	48	53	43	70	10	45	2.4	10	63	7.6
Eu/Eu*	1.1	1.1	1.1	0.99	10	1.1	0.07	10	1.0	0.06

Eu/Eu* = $Eu_{cn}/[(Sm_{cn})(Gd_{cn})]^{1/2}$.
Subscript $_{cn}$ refers to chondrite-normalized values (McDonough and Sun, 1995).
Numbers were rounded following the procedure given by Verma (2005).

Figure 7. Th/U versus Th bivariate plot for the beach sands.

Figure 6. Chondrite-normalized rare earth elements plot. Normalization values are from McDonough and Sun (1995). The average upper continental crust (UCC; Taylor and McLennan, 1985) value is also included for reference. **a)** San Nicolás; **b)** San Carlos.

kaolinite, illite, and muscovite show values of <0.84 (Cox et al., 1995; Cullers, 2000). The ICV values of SN (ca. 1.08–2.18) and SC sands (ca. 1.77–2.87) are higher than 0.84, indicating that they are enriched in rock-forming minerals (Table 2). Similarly, the SiO_2/Al_2O_3 ratio can be used to understand the textural maturity of sediments, where a high value represents compositionally matured sediments (e.g., Ahmad and Chandra, 2013). The SiO_2/Al_2O_3 ratios vary from 6.31 to 7.03 and 5.54 to 5.76 in the medium- and fine-grained SN sands, respectively, whereas, they are 4.75–5.07 and 4.32–4.85 for the medium- and fine-grained SC sands, respectively (Table 2). The higher SiO_2/Al_2O_3 ratio of the medium- and fine-grained SN sands than that in the SC sands indicates that the compositional maturity is greater for the SN sands (F_{calc} = 366.756151 > (F_{crit})$_{99\%}$ = 5.065158; Table 1).

In addition, a statistically significant positive correlation of Zr with Yb (r = 0.90, n = 10) and HREEs (r

= 0.62, n = 10; critical t value for 99% confidence level is 0.708; Verma, 2005) for the fine-grained SN sands indicates that the HREE fractionation is controlled mostly by the concentration of zircon mineral, whereas the correlation is not statistically significant for Zr against Yb and HREEs for the medium-grained SN (r = 0.27 and 0.01, respectively, n = 10) and SC (r = –0.43 and –0.76, respectively, n = 10) sands, which reveals that these elements were not influenced by zircon mineral. The SEM-EDS study also showed a zirconium-rich composition for the fine-grained SN sand (Figure 4b). In general, the results suggest that the SN sands are largely influenced by hydraulic sorting and indicate high maturity. This observation is consistent with the modal framework composition (Table 3).

5.3. Provenance

The geochemical compositions of terrigenous sediments are frequently used by many researchers to infer the provenance, because they tend to reflect source rock composition (Al-Juboury and Al-Hadidy, 2009; Bakkiaraj et al., 2010; Shadan and Hosseini-Barzi, 2013). Elements concentrated in mafic (Sc, Cr, and Co) and in silicic (La, Th, and REE) sediments, REE patterns, and the size of the Eu anomaly have been used extensively for provenance interpretation (e.g., Shynu et al., 2011). The major element-based provenance discriminant function diagram of Roser and Korsch (1988) is frequently used by many researchers to identify the provenance of terrigenous sediments (Madhavaraju and Lee, 2010; Hofer et al., 2013; Khanchuk et al., 2013; Vdačný et al., 2013). This diagram discriminates 4 major provenance categories of mafic (P1), intermediate (P2), felsic (P3), and quartzose recycled (P4). This discriminant function diagram indicates a felsic source for SN and intermediate source for SC sands (Figure 8). We also note that although this diagram is based on discriminant functions, it does not fully take into account
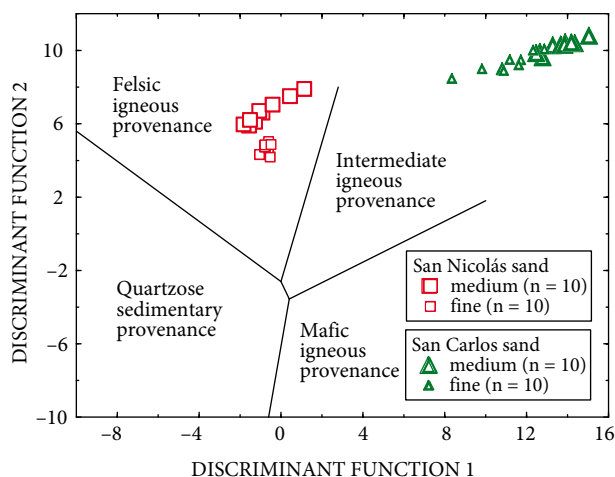
Figure 8. Major element provenance discriminant function diagram for the beach sands (Roser and Korsch, 1988). The discriminant functions are: discriminant function 1 = $(-1.773 \times TiO_2) + (0.607 \times Al_2O_3) + (0.760 \times Fe_2O_3) + (-1.500 \times MgO) + (0.616 \times CaO) + (0.509 \times Na_2O) + (-1.224 \times K_2O) + (-9.090)$; discriminant function 2 = $(0.445 \times TiO_2) + (0.070 \times Al_2O_3) + (-0.250 \times Fe_2O_3) + (-1.142 \times MgO) + (0.438 \times CaO) + (1.475 \times Na_2O) + (1.426 \times K_2O) + (-6.861)$.

the recommendations of Aitchison (1986) as done by Verma et al. (2006) for the first time for such applications in geosciences (see also Agrawal and Verma, 2007; Verma et al., 2013b; Verma and Armstrong-Altrin, 2013).

The K_2O and Rb contents in terrigenous sediments are sensitive to sedimentary recycling processes and have been widely used as indicators for source composition (Armstrong-Altrin et al., 2012; Tao et al., 2013). The $K_2O/$
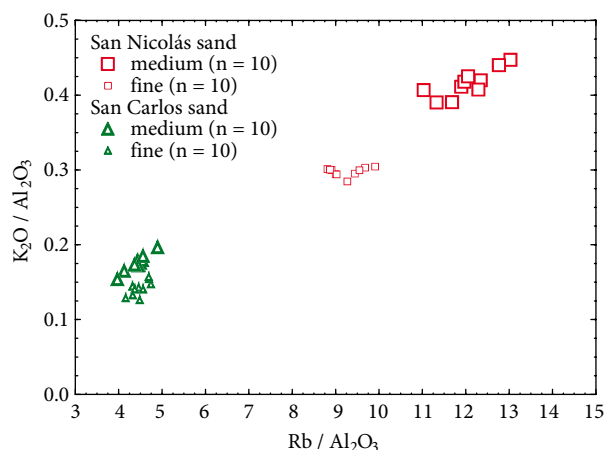
Figure 9. K_2O/Al_2O_3 versus Rb/Al_2O_3 bivariate diagram for the beach sands.

Al_2O_3 versus Rb/Al_2O_3 bivariate plot (Figure 9) reveals a compositional difference between the SN and SC sands and these ratios are higher in the SN sands (Table 1). This variation may reflect changing average source rock compositions from felsic to intermediate, respectively. Elevated values of Cr (>150 ppm) and Ni (>100 ppm) are diagnostic of ultramafic sources (Garver et al., 1996). The SN and SC sands have low average Cr (ca. 5–20 and 6–13, respectively) and Ni (ca. 4–14 and 6–8, respectively) contents. These low Cr and Ni values exclude the existence of ultramafic rocks in the source area.

Trace element ratios such as Eu/Eu*, $(La/Lu)_{cn}$, La/Sc, La/Co, Th/Sc, Th/Co, and Th/Cr are significantly different in mafic and felsic source rocks (Cullers, 2000) and can therefore provide information about the provenance of

Table 6. Range of elemental ratios of beach sands in this study compared to the ratios in similar fractions derived from felsic and mafic rocks.

Elemental Ratio	San Nicolás beach sands[1]		San Carlos beach sands[1]		Range of sediment from felsic sources[2]	Range of sediment from mafic sources[2]
	Medium	Fine	Medium	Fine		
Eu/Eu*	0.83–0.92	0.81–0.06	0.99–1.22	0.94–1.1	0.40–0.94	0.71–0.95
$(La/Lu)_{cn}$	8.7–10	8.5–9.8	7.98–9.31	8.6–11.3	3.00–27	1.10–7
La/Sc	8.4–10.6	5.4–6	3.39–9.98	3.1–14.8	2.50–16.3	0.43–0.86
La/Co	6.8–8.2	5.0–6	3.75–4.67	4.1–6	1.80–13.8	0.14–0.38
Th/Sc	2.8–3.5	1.7–2	0.97–3.27	0.77–3.5	0.84–20.5	0.05–0.22
Th/Co	2.3–2.8	1.6–1.8	1.02–1.55	1.02–1.73	0.67–19.4	0.04–1.4
Th/Cr	0.62–0.91	0.40–0.48	0.29–0.49	0.23–0.36	0.13–2.7	0.02–0.05

[1]This study.
[2]Cullers (1994, 2000); Cullers and Podkovyrov (2000).
Eu/Eu* = $Eu_{cn}/[(Sm_{cn})(Gd_{cn})]^{1/2}$.
Subscript $_{cn}$ refers to chondrite-normalized values (McDonough and Sun, 1995).

terrigenous sediments (Armstrong-Altrin et al., 2004, 2013; Nagarajan et al., 2007). These ratios are compared in Table 6 with sediments derived from mafic and felsic source rocks. This comparison reveals that most of the trace element ratios of the SN sands fall within the range of sediments derived from felsic rocks (Table 6), except the Th/Co ratio of SC sands, which is comparable to sediments derived from mafic rocks. The REE patterns and the range in Eu anomalies have been used extensively to study the source of terrigenous sediments (e.g., Etemad-Saeed et al., 2011) since mafic igneous rocks contain low LREE/HREE ratios and little or no negative Eu anomalies, whereas felsic igneous rocks generally possess higher LREE/HREE ratios and negative Eu anomalies (Cullers et al., 1987). In the studied samples, the total REE contents of the medium-grained sands are depleted and they are enriched in the fine-grained sands, and the shapes of the REE patterns for SN and SC sands are similar, except for the Eu anomaly. The significant enrichment of the LREEs and the flat HREE patterns of the SN sands suggest that the sources were largely felsic rocks. A negative Eu anomaly is recorded in the SN sands (Eu/Eu* = 0.83 ± 0.03 and 0.81 ± 0.06 for the medium- and fine-grained sands, respectively), whereas few SC sands show a low positive Eu anomaly (Table 5). The low positive Eu anomaly in the SC sands is likely because of the contribution of sediments from the intermediate rocks (e.g., andesite).

In addition, to identify the provenance, the average REE data of the source rocks located relatively adjacent to the beach areas were compared with the beach sand geochemistry of the present study (Figure 10). The compiled rock types include rhyolite, granite, andesite, and basalt exposed along the coastal and central areas of Sonora (Nos. 1–9; Figure 1). The average REE patterns of
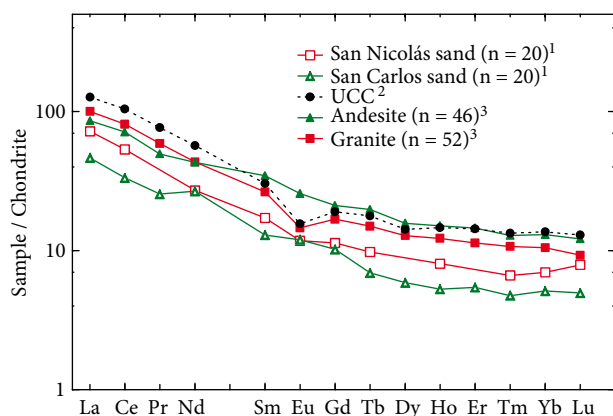
Figure 10. Average chondrite-normalized REE patterns for the beach sands. Normalization values are from McDonough and Sun (1995). n = number of samples; UCC = upper continental crust; [1]this study; [2]Taylor and McLennan (1985). [3]Andesite and granite were compiled from source areas 1–9 as shown in Figure 1.
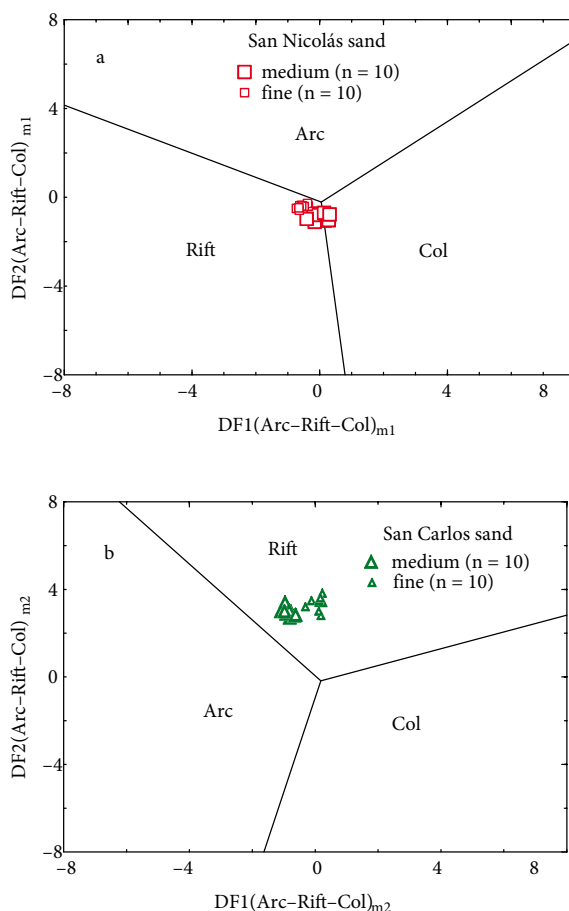
Figure 11. a) Discriminant function multidimensional diagram for high-silica clastic sediments (Verma and Armstrong-Altrin, 2013). The subscript $_{m1}$ in DF1 and DF2 represents the high-silica diagram based on $\log_e$-ratios of major elements. The discriminant function equations are: $DF1_{(Arc-Rift-Col)m1} = (-0.263 \times \ln(TiO_2/SiO_2)_{adj}) + (0.604 \times \ln(Al_2O_3/SiO_2)_{adj}) + (-1.725 \times \ln(Fe_2O_3^t/SiO_2)_{adj}) + (0.660 \times \ln(MnO/SiO_2)_{adj}) + (2.191 \times \ln(MgO/SiO_2)_{adj}) + (0.144 \times \ln(CaO/SiO_2)_{adj}) + (-1.304 \times \ln(Na_2O/SiO_2)_{adj}) + (0.054 \times \ln(K_2O/SiO_2)_{adj}) + (-0.330 \times \ln(P_2O_5/SiO_2)_{adj}) + 1.588$. $DF2_{(Arc-Rift-Col)m1} = (-1.196 \times \ln(TiO_2/SiO_2)_{adj}) + (1.604 \times \ln(Al_2O_3/SiO_2)_{adj}) + (0.303 \times \ln(Fe_2O_3^t/SiO_2)_{adj}) + (0.436 \times \ln(MnO/SiO_2)_{adj}) + (0.838 \times \ln(MgO/SiO_2)_{adj}) + (-0.407 \times \ln(CaO/SiO_2)_{adj}) + (1.021 \times \ln(Na_2O/SiO_2)_{adj}) + (-1.706 \times \ln(K_2O/SiO_2)_{adj}) + (-0.126 \times \ln(P_2O_5/SiO_2)_{adj}) - 1.068$. **b)** Discriminant function multidimensional diagram for low-silica clastic sediments (Verma and Armstrong-Altrin, 2013). The subscript $_{m2}$ in DF1 and DF2 represents the low-silica diagram based on $\log_e$-ratio of major elements. Discriminant function equations are: $DF1_{(Arc-Rift-Col)m2} = (0.608 \times \ln(TiO_2/SiO_2)_{adj}) + (-1.854 \times \ln(Al_2O_3/SiO_2)_{adj}) + (0.299 \times \ln(Fe_2O_3^t/SiO_2)_{adj}) + (-0.550 \times \ln(MnO/SiO_2)_{adj}) + (0.120 \times \ln(MgO/SiO_2)_{adj}) + (0.194 \times \ln(CaO/SiO_2)_{adj}) + (-1.510 \times \ln(Na_2O/SiO_2)_{adj}) + (1.941 \times \ln(K_2O/SiO_2)_{adj}) + (0.003 \times \ln(P_2O_5/SiO_2)_{adj}) - 0.294$. $DF2_{(Arc-Rift-Col)m2} = (-0.554 \times \ln(TiO_2/SiO_2)_{adj}) + (-0.995 \times \ln(Al_2O_3/SiO_2)_{adj}) + (1.765 \times \ln(Fe_2O_3^t/SiO_2)_{adj}) + (-1.391 \times \ln(MnO/SiO_2)_{adj}) + (-1.034 \times \ln(MgO/SiO_2)_{adj}) + (0.225 \times \ln(CaO/SiO_2)_{adj}) + (0.713 \times \ln(Na_2O/SiO_2)_{adj}) + (0.330 \times \ln(K_2O/SiO_2)_{adj}) + (0.637 \times \ln(P_2O_5/SiO_2)_{adj}) - 3.631$.

rhyolite and basalt are not provided in Figure 10, because their patterns are different from the SN and SC sands. The general shapes of the REE pattern of SN sands are similar to that of granite rock. Similarly, the REE pattern of the San Carlos sands shows a closer resemblance to that of andesite rock. This comparison reveals that the SN sands received a major contribution from felsic rocks and SC sands from intermediate rocks. The source discrimination between the 2 beach areas also reveals that the role of longshore current in mixing and homogenization of sands is not significant along the coastal region of our study areas.

5.4. Tectonic setting

The discrimination diagrams proposed by Bhatia (1983) and Roser and Korsch (1986) have mostly been used to identify the tectonic setting of unknown basins (Jafarzadeh et al., 2013; Nowrouzi et al., 2013; Tetiker, 2014). These diagrams, though widely used ever since their proposal, do not incorporate a coherent statistical treatment of compositional data (Thomas and Aitchison, 2005; Agrawal and Verma, 2007; Verma, 2010, 2012; Verma and Armstrong-Altrin, 2013). On the other hand, the use of these conventional discrimination diagrams has been cautioned against by many researchers (e.g., Armstrong-Altrin and Verma, 2005; Ryan and Williams, 2007). Armstrong-Altrin and Verma (2005) evaluated these major element-based discrimination diagrams using Miocene to Recent sediments and showed a low percentage success rate (0%–23%) for the Bhatia (1983) diagram and ~31.5%–52.3% for the Roser and Korsch (1986) diagram.

Recently, Verma and Armstrong-Altrin (2013) proposed 2 discriminant function-based major element diagrams for the tectonic discrimination of siliciclastic sediments from 3 main tectonic settings: island or continental arc, continental rift, and collision, created for the tectonic discrimination of high-silica [$(SiO_2)_{adj}$ = 63%–95%] and low-silica rocks [$(SiO_2)_{adj}$ = 35%–63%]. These 2 diagrams were constructed based on worldwide examples of Neogene-Quaternary siliciclastic sediments from known tectonic settings, $\log_e$-ratio transformation of 10 major elements with SiO_2 as the common denominator, and linear discriminant analysis of the $\log_e$-transformed ratio data. Recently, these diagrams were evaluated by Armstrong-Altrin (2014), who suggested that these diagrams can be considered as a useful tool for successfully discriminating the tectonic setting of older sedimentary basins, which may consist of one or more tectonic assemblages. These discriminant function-based major element diagrams (Figures 11a and 11b) were used in this study to identify

the tectonic environment of the 2 beach areas, i.e. the high-silica diagram [$(SiO_2)_{adj}$ = >63% to ≤95%] for the SN sand and the low-silica diagram [$(SiO_2)_{adj}$ = >35% to ≤63%] for the SC sand. In the high-silica diagram (Figure 11a), most of the samples plotted in the rift field, except 4 samples that plotted near the line between the collision and rift fields. In the low-silica diagram (Figure 11b), all samples plotted in the area assigned for the rift field. The results obtained from these 2 discriminant function-based multidimensional diagrams provide good evidence for the Gulf of California rift system, which is consistent with the general geology of Mexico (Morán-Zenteno, 1994).

The results of this study demonstrate that the fine-grained sands of the 2 beach areas were enriched in trace element concentrations, especially in REEs and high field strength elements, indicating the accumulation of heavy minerals in fine-grained sediments due to hydraulic sorting. The compositional difference between the fine-grained SN and fine-grained SC sands further demonstrates that chemical discrimination depends not only on mean grain size, but also on the source rock composition in controlling the chemistry of the derived sediments. The comparison of REE patterns to the source rocks revealed that the SN and SC sands received sediments from felsic (granite) and intermediate (andesite) rocks, respectively. The results of this study provide evidence for the extension in the Gulf of California rift system.

References

Agrawal S, Verma SP (2007). Comment on "Tectonic classification of basalts with classification trees" by Pieter Vermeesch (2006). Geochim Cosmochim Ac 71: 3388–3390.

Ahmad I, Chandra R (2013). Geochemistry of loess-paleosol sediments of Kashmir Valley, India: provenance and weathering. J Asian Earth Sci 66: 73–89.

Aitchison J (1986). The Statistical Analysis of Compositional Data. London, UK: Chapman and Hall.

Al-Juboury AI, Al-Hadidy AH (2009). Petrology and depositional evolution of the Palaeozoic rocks of Iraq. Mar Petrol Geol 26: 208–231.

Allen JL, Johnson CL, Heumann MJ, Gooley J, Gallin W (2012). New technology and methodology for assessing sandstone composition: a preliminary case study using a quantitative electron microscope scanner (QEMScan). In: Rasbury ET, Hemming SR, Riggs NR, editors. Mineralogical and Geochemical Approaches to Provenance. Geological Society of America Special Paper 487: 177–194.

Armstrong-Altrin JS (2009). Provenance of sands from Cazones, Acapulco, and Bahía Kino beaches, Mexico. Rev Mex Cien Geol 26: 764–782.

Armstrong-Altrin JS (2014). Evaluation of two multidimensional discrimination diagrams from beach and deep-sea sediments from the Gulf of Mexico and their application to Precambrian clastic sedimentary rocks. Int Geol Rev DOI 10.1080/00206814.2014.936055 (in press).

Armstrong-Altrin JS, Lee YI, Kasper-Zubillaga JJ, Carranza-Edwards A, Garcia D, Eby N, Balaram V, Cruz-Ortiz NL (2012). Geochemistry of beach sands along the Western Gulf of Mexico, Mexico: implication for provenance. Chem Erde Geochem 72: 345–362.

Armstrong-Altrin JS, Lee YI, Verma SP, Ramasamy S (2004). Geochemistry of sandstones from the Upper Miocene Kudankulam Formation, southern India: implications for provenance, weathering, and tectonic setting. J Sediment Res 74: 285–297.

Armstrong-Altrin JS, Nagarajan R, Madhavaraju J, Rosalez-Hoz L, Lee YI, Balaram V, Cruz-Martinez A, Avila-Ramirez G (2013). Geochemistry of the Jurassic and upper Cretaceous shales from the Molango Region, Hidalgo, Eastern Mexico: Implications of source-area weathering, provenance, and tectonic setting. CR Geosci 345: 185–202.

Armstrong-Altrin JS, Natalhy-Pineda O (2013). Microtextures of detrital sand grains from the Tecolutla, Nautla, and Veracruz beaches, western Gulf of Mexico, Mexico: implications for depositional environment and palaeoclimate. Arab J Geosci DOI 10.1007/s12517-013-1088-x (in press).

Armstrong-Altrin JS, Verma SP (2005). Critical evaluation of six tectonic setting discrimination diagrams using geochemical data of Neogene sediments from known tectonic setting. Sediment Geol 177: 115–129.

Bakkiaraj D, Nagendra R, Nagarajan R, Armstrong-Altrin JS (2010). Geochemistry of sandstones from the Upper Cretaceous Sillakkudi Formation, Cauvery Basin, Southern India: Implication for provenance. J Geol Soc India 76: 453–467.

Bhatia MR (1983). Plate tectonics and geochemical composition of sandstones. J Geol 91: 611–627.

Carriquiry JD, Sánchez A (1999). Sedimentation in the Colorado River delta and Upper Gulf of California after nearly a century of discharge loss. Mar Geo 158: 125–145.

Concepcion RAB, Dimalanta CB, Yumul GP, Faustino-Eslava DV, Queaño KL, Tamayo RA, Imai A (2012). Petrography, geochemistry, and tectonics of a rifted fragment of Mainland Asia: evidence from the Lasala Formation, Mindoro Island, Philippines. Int J Earth Sci 101: 273–290.

Conly AG, Brenan JM, Bellon H, Scott SD (2005). Arc to rift transitional volcanism in the Santa Rosalía Region, Baja California Sur, Mexico. J Volcanol Geoth Res 142: 303–341.

Cox R, Lowe DR, Cullers RL (1995). The influence of sediment recycling and basement composition on evolution of mudrock chemistry in the southwestern United States. Geochim Cosmochim Ac 59: 2919–2940.

Cruz-Huicochea R, Verma SP (2013). New critical values for F and their use in the ANOVA and Fisher's F tests for evaluating data of geochemical reference material granite G-2 (U.S.A.) and igneous rocks from the Eastern Alkaline Province (Mexico). J Iber Geol 39: 13–30.

Cullers RL (1994). The controls on the major and trace element variation of shales, siltstones, and sandstones of Pennsylvanian-Permian age from uplifted continental blocks in Colorado to platform sediment in Kansas, USA. Geochim Cosmochim Ac 58: 4955–4972.

Cullers RL (2000). The geochemistry of shales, siltstones and sandstones of Pennsylvanian - Permian age, Colorado, U.S.A.: Implications for provenance and metamorphic studies. Lithos 51: 181–203.

Cullers RL, Barrett T, Carlson R, Robinson B (1987). Rare earth element and mineralogic changes in Holocene soil and stream sediment: a case study in the Wet Mountains, Colorado, USA. Chem Geol 63: 275–297.

Cullers RL, Chaudhuri S, Kilbane N, Koch R (1979). Rare earths in size fractions and sedimentary rocks of Pennsylvanian-Permian age from the mid-continent of the USA. Geochim Cosmochim Ac 43: 1285–1302.

Cullers RL, Podkovyrov VN (2000). Geochemistry of the Mesoproterozoic Lakhanda shales in southeastern Yakutia, Russia: implications for mineralogical and provenance control, and recycling. Precambrian Res 104: 77–93.

Deepthi K, Natesan U, Muthulakshmi AL, Ferrer VA, Venugopalan VP, Narasimhan SV (2013). Geochemical characteristics and depositional environment of Kalpakkam, southeast coast of India. Environ Earth Sci 69: 2357–2364.

Desonie DL (1992). Geologic and geochemical reconnaissance of Isla San Esteban: post-subduction orogenic volcanism in the Gulf of California. J Volcanol Geoth Res 52: 123–140.

Dickinson WR, Beard LS, Brakenridge GR, Erjavec JL, Ferguson RC, Inman KF, Knepp RA, Lindberg FA, Ryberg PT (1983). Provenance of North American Phanerozoic sandstones in relation to tectonic setting. Geol Soc Am Bull 94: 222–235.

Effoudou-Priso EN, Onana VL, Boubakar L, Beyala VKK, Ekodeck GE (2014). Relationships between major and trace elements during weathering processes in a sedimentary context: implications for the nature of source rocks in Douala, Littoral Cameroon. Chem Erde Geochem DOI 10.1016/j.chemer.2014.05.003 (in press).

Etemad-Saeed N, Hosseini-Barzi M, Armstrong-Altrin JS (2011). Petrography and geochemistry of clastic sedimentary rocks as evidence for provenance of the Lower Cambrian Lalun Formation, Posht-e-badam block, Central Iran. J Afr Earth Sci 61: 142–159.

Folk RL (1966). A review of grain-size parameters. Sedimentology 6: 73–96.

Folk RL, Ward WC (1957). Brazos River Bar, a study in the significance of grain-size parameters. J Sediment Petrol 27: 3–26.

Garver JI, Royce PR, Smick TA (1996). Chromium and nickel in shale of the Taconic Foreland: a case study for the provenance of fine-grained sediments with an ultramafic source. J Sediment Res 66: 100–106.

Greenough JD, Fryer BJ, Robinson PT (1990). Geochemical effects of alteration on mafic rocks from Indian Ocean Site 706. In: Duncan RA, Backman J, Peterson LC, editors. Proceedings of the Ocean Drilling Program, Scientific Results 115: 85–92.

Grisby JD (1990). Detrital magnetite as a provenance indicator. J Sediment Petrol 60: 940–951.

Hofer G, Wagreich M, Neuhuber S (2013). Geochemistry of fine-grained sediments of the Upper Cretaceous to Paleogene Gosau Group (Austria, Slovakia): implications for paleoenvironmental and provenance studies. Geosci Front 4: 449–468.

Hofmann A, Harris C (2008). Silica alteration zones in the Barberton greenstone belt: a window into subseafloor processes 3.5-3.3 Ga ago. Chem Geo 257: 224–242.

Hossain HMZ, Roser BP, Kimura JI (2010). Petrography and whole-rock geochemistry of the Tertiary Sylhet succession, northeastern Bengal Basin, Bangladesh: provenance and source area weathering. Sediment Geol 228: 171–183.

Hossain HMZ, Tarek M, Armstrong-Altrin JS, Monir MU, Ahmed MT, Ahmed SI, Hernandez-Coronado CJ (2014). Microtextures of detrital sand grains from the Cox's Bazar beach, Bangladesh: Implications for provenance and depositional environment. Carpath J Earth Env 9: 187–197.

Ingersoll RV, Bulard TF, Ford RL, Grimn JP, Pickle JP, Sares SW (1984). The effect of grain size on detrital modes: a test of the Gazzi-Dickinson point counting method. J Sediment Petrol 54: 103–116.

Jafarzadeh M, Harami RM, Amini A, Mahboubi A, Farzaneh F (2013). Geochemical constraints on the provenance of Oligocene-Miocene siliciclastic deposits (Zivah Formation) of NW Iran: implications for the tectonic evolution of the Caucasus. Arab J Geosci DOI 10.1007/s12517-013-1018-y (in press).

Jarvis KE (1988). Inductively coupled plasma mass spectrometry: A new technique for the rapid or ultra-trace level determination of the rare-earth elements in geological materials. Chem Geol 68: 31–39.

Kasper-Zubillaga JJ, Acevedo-Vargas B, Morton Bermea O, Ortiz-Zamora G (2008a). Rare earth elements of the Altar desert dune and coastal sands, Northwestern Mexico. Chem Erde Geochem 68: 45–59.

Kasper-Zubillaga JJ, Carranza-Edwards A, Morton-Bermea O (2008b). Heavy minerals and rare earth elements in coastal and inland dune sands of El Vizcaino Desert, Baja California Peninsula, Mexico. Mar Georesour Geotec 26: 172–188.

Khanchuk AI, Nevstruev VG, Berdnikov NV, Nechaev VP (2013). Petrochemical characteristics of carbonaceous shales in the eastern Bureya massif and their precious-metal mineralization. Russ Geol Geophys 54: 627–636.

Lozano R, Bernal JP (2005). Characterization of a new set of eight geochemical reference materials for XRF major and trace element analysis. Rev Mex Cien Geol 22: 329–344.

Madhavaraju J, Lee YI (2010). Influence of Deccan volcanism in the sedimentary rocks of Late Maastrichtian-Danian age of Cauvery basin Southeastern India: constraints from geochemistry. Curr Sci India 98: 528–537.

Marsaglia KM (1991). Provenance of sands and sandstones from a rifted continental arc, Gulf of California, Mexico. In: Fisher RV, Smith GA, editors. Sedimentation in Volcanic Settings. Tulsa, OK, USA: Society for Sedimentary Geology Special Publications, pp. 237–248.

McDonough WF, Sun SS (1995). The composition of the Earth. Chem Geol 120: 223–253.

McLennan SM, Hemming S, McDaniel DK, Hanson GN (1993). Geochemical approaches to sedimentation, provenance, and tectonics. In: Johnsson MJ, Basu A, editors. Processes Controlling the Composition of Clastic Sediments. Boulder, CO, USA: Geological Society of America, Special Paper, pp. 21–40.

Morán-Zenteno D (1994). The Geology of the Mexican Republic. AAPG Studies in Geology. Tulsa, OK, USA: American Association of Petroleum Geologists.

Nagarajan R, Madhavaraju J, Nagendra R, Armstrong-Altrin JS, Moutte J (2007). Geochemistry of Neoproterozoic shales of Rabanpalli formation, Bhima basin, northern Karnataka, southern India: implications for provenance and paleoredox conditions. Rev Mex Cien Geol 24: 150–160.

Nardi LVS, Formoso MLL, Müller IF, Fontana E, Jarvis K, Lamarão C (2013). Zircon/rock partition coefficients of REEs, Y, Th, U, Nb, and Ta in granitic rocks: uses for provenance and mineral exploration purposes. Chem Geol 335: 1–7.

Nesbitt HW, Young GM (1982). Early Proterozoic climates and plate motions inferred from major element chemistry of lutites. Nature 299: 715–717.

Nowrouzi Z, Moussavi-Harami R, Mahboubi A, Gharaie MHM, Ghaemi F (2013). Petrography and geochemistry of Silurian Niur sandstones, Derenjal Mountains, East Central Iran: implications for tectonic setting, provenance and weathering. Arab J Geosci DOI 10.1007/s12517-013-0912-7 (in press).

Ohta T (2008). Measuring and adjusting the weathering and hydraulic sorting effects for rigorous provenance analysis of sedimentary rocks: a case study from the Jurassic Ashikita Group, south-west Japan. Sedimentology 55: 1687–1701.

Paz-Moreno FA, Demant A (1999). The Recent Isla San Luis volcanic centre: petrology of a rift-related volcanic suite in the northern Gulf of California, Mexico. J Volcanol Geoth Res 93: 31–52.

Ramos-Velázquez E, Calmus T, Valencia V, Iriondo A, Valencia-Moreno M, Bellon H (2008). U-Pb and ^{40}Ar/^{39}Ar geochronology of the coastal Sonora batholith: New insights on Laramide continental arc magmatism. Rev Mex Cien Geol 25: 314–333.

Roldán-Quintana J, McDowell FW, Delgado-Granados H, Valencia-Moreno M (2009). East-west variations in age, chemical and isotopic composition of the Laramide batholith in southern Sonora, Mexico. Rev Mex Cien Geol 26: 543–563.

Roser BP, Korsch RJ (1986). Determination of tectonic setting of sandstone-mudstone suites using SiO_2 content and K_2O/Na_2O ratio. J Geol 94: 635–650.

Roser BP, Korsch RJ (1988). Provenance signatures of sandstone-mudstone suites determined using discrimination function analysis of major element data. Chem Geol 67: 119–139.

Ryan KM, Williams DM (2007). Testing the reliability of discrimination diagrams for determining the tectonic depositional environment of ancient sedimentary basins. Chem Geol 242: 103–125.

Saunders AD (1983). Geochemistry of basalts recovered from the Gulf of California during Leg 65 of the Deep Sea Drilling Project. In: Lewis BTR, Robinson P, editors. Initial Reports of the Deep Sea Drilling Project. College Station, TX, USA: Texas A & M University Ocean Drilling Program, pp. 591–621.

Saunders AD, Fornari DJ, Joron JL, Tarney J, Treuil M (1982). Geochemistry of basic igneous rocks, Gulf of California, Initial Reports of the Deep Sea Drilling Project Leg 64. In: Curray JR, Moore DG, editors. Initial Reports of the Deep Sea Drilling Project. College Station, TX, USA: Texas A & M University Ocean Drilling Program, pp. 595–642.

Selvaraj K, Chen CTA (2006). Moderate chemical weathering of subtropical Taiwan: constraints from solid-phase geochemistry of sediments and sedimentary rocks. J Geol 14: 101–116.

Shadan M, Hosseini-Barzi M (2013). Petrography and geochemistry of the Ab-e-Haji Formation in central Iran: implications for provenance and tectonic setting in the southern part of the Tabas block. Rev Mex Cien Geol 30: 80–95.

Shynu R, Rao VP, Kessarkar PM, Rao TG (2011). Rare earth elements in suspended and bottom sediments of the Mandovi estuary, central west coast of India: Influence of mining. Estuar Coast Shelf S 94: 355–368.

Singh P (2009). Major, trace and REE geochemistry of the Ganga River sediments: influence of provenance and sedimentary processes. Chem Geol 266: 242–255.

Srivastava AK, Randive KR, Khare N (2013). Mineralogical and geochemical studies of glacial sediments from Schirmacher Oasis, East Antarctica. Quatern Int 292: 205–216.

Sun L, Gui H, Chen S (2013). Geochemistry of sandstones from the Neoproterozoic Jinshanzhai Formation in northern Anhui Province, China: Provenance, weathering and tectonic setting. Chin J Geochem 32: 95–103.

Suttner LJ, Basu A (1985). The effect of grain size on detrital modes: a test of the Gazzi-Dickinson point-counting method - Discussion. J Sediment Petrol 55: 616–617.

Tao H, Wang Q, Yang X, Jiang L (2013). Provenance and tectonic setting of Late Carboniferous clastic rocks in west Junggar, Xinjiang, China: a case from the Hala-alat Mountains. J Asian Earth Sci 64: 210–222.

Taylor SR, McLennan SM (1985). The Continental Crust: Its Composition and Evolution. Oxford, UK: Blackwell.

Tetiker S (2014). Petrography and geochemistry of Early Palaeozoic clastic rocks from the southeast Anatolian autochthone rocks in Mardin area (Derik-Kiziltepe), Turkey. Carpath J Earth Env 9: 149–162.

Thomas CW, Aitchison J (2005). Compositional data analysis of geological variability and process: a case study. Mathem Geol 37: 753–772.

Till CB, Phillip BG, Spera FJ, MacMillan I, Blair KD (2009). Perils of petrotectonic modelling: a view from southern Sonora, Mexico. J Volcanol Geoth Res 186: 160–168.

Torres-Alvarado IS, Pandarinath K, Verma SP, Dulski P (2007). Mineralogical and geochemical effects due to hydrothermal alteration in the Los Azufres geothermal field, Mexico. Rev Mex Cien Geol 24: 15–24.

Valencia-Moreno M, Ruiz J, Barton MD, Patchett PJ, Zuürcher L, Hodkinson DG, Roldán-Quintana J (2001). A chemical and isotopic study of the Laramide granitic belt of north western Mexico: Identification of the southern edge of the North American Precambrian basement. Geol Soc Am Bull 113: 1409–1422.

Valencia-Moreno M, Ruiz J, Ochoa-Landín L, Martínez-Serrano R, Vargas-Navarro P (2003). Geochemistry of the coastal Sonora batholith, north-western Mexico. Can J Earth Sci 40: 819–831.

Vdačný M, Vozárová A, Vozár J (2013). Geochemistry of the Permian sandstones from the Malužiná Formation in the Malé Karpaty Mts (Hronic Unit, Western Carpathians, Slovakia): implications for source-area weathering, provenance and tectonic setting. Geol Carpath 64: 23–38.

Verma SP (1992). Seawater alteration effects on REE, K, Rb, Cs, Sr, U, Th, Pb and Sr-Nd-Pb isotope systematics of Mid-Ocean Ridge Basalt. Geochem J 26: 159–177.

Verma SP (2005). Estadística Básica para el Manejo de Datos Experimentales: Aplicación a la Geoquímica (Geoquimiometría). Mexico City, Mexico: National Autonomous University of Mexico (in Spanish).

Verma SP (2010). Statistical evaluation of bivariate, ternary and discriminant function tectonomagmatic discrimination diagrams. Turkish J Earth Sci 19: 185–238.

Verma SP (2012). Geochemometrics. Rev Mex Cien Geol 29: 276–298.

Verma SP, Armstrong-Altrin JS (2013). New multi-dimensional diagrams for tectonic discrimination of siliciclastic sediments and their application to Precambrian basins. Chem Geol 355: 117–133.

Verma SP, Cruz-Huicochea R (2013). Alternative approach for precise and accurate Student's t critical values and application in geosciences. J Iber Geol 39: 31–56.

Verma SP, Cruz-Huicochea R, Díaz-González L (2013a). Univariate data analysis system: deciphering mean compositions of island and continental arc magmas, and influence of the underlying crust. Int Geol Rev 55: 1922–1940.

Verma SP, Díaz-González L (2012). Application of the discordant outlier detection and separation system in the Geosciences. Int Geol Rev 54: 593–614.

Verma SP, Guevara M, Agrawal S (2006). Discriminating four tectonic settings: five new geochemical diagrams for basic and ultrabasic volcanic rocks based on log-ratio transformation of major-element data. J Earth Syst Sci 115: 485–528.

Verma SP, Pandarinath K, Verma SK, Agrawal S (2013b). Fifteen new discriminant-function-based multi-dimensional robust diagrams for acid rocks and their application to Precambrian rocks. Lithos 168-169: 113–123.

Verma SP, Torres-Alvarado, IS, Satir M, Dobson P (2005). Hydrothermal alteration effects in geochemistry and Sr, Nd, Pb, and O isotopes of magmas from Los Azufres geothermal field, Mexico: a statistical approach. Geochem J 39: 141–163.

Vidal-Solano JR, Paz-Moreno FA, Demant A, López-Martínez M (2007). Ignimbritas hiperalcalinas del Mioceno medio en Sonora Central: revaluación de la estratigrafía y significado del volcanismo terciario. Rev Mex Cien Geol 24: 47–67 (in Spanish).

Weltje GJ (2006). Ternary sandstone composition and provenance: an evaluation of the Dickinson Model. In: Buccianti A, Mateu-Figueras G, Pawlowsky-Glahn V, editors. Compositional Data Analysis in the Geosciences: From Theory to Practice. Geological Society of London Special Publications 264: 79–99.

Wu W, Zheng H, Xu S, Yang J, Liu W (2013). Trace element geochemistry of riverbed and suspended sediments in the upper Yangtze River. J Geochem Explor 124: 67–78.

Young SM, Pitawala A, Ishiga H (2013). Geochemical characteristics of stream sediments, sediment fractions, soils, and basement rocks from the Mahaweli River and its catchment, Sri Lanka. Chem Erde Geochem 73: 357–371.

Zaid SM (2013). Provenance, diagenesis, tectonic setting and reservoir quality of the sandstones of the Kareem Formation, Gulf of Suez, Egypt. J Afr Earth Sci 85: 31–52.

Zhang YL, Wang ZQ, Yan Z, Wan T (2011). Tectonic setting of Neoproterozoic Beiyixi Formation in Quruqtagh area, Xinjiang: evidence from geochemistry of clastic rocks. Acta Petrol Sin 27: 1785–1796.